ANALYSES RELATED TO THE HUGHES GYROSTAT SYSTEM

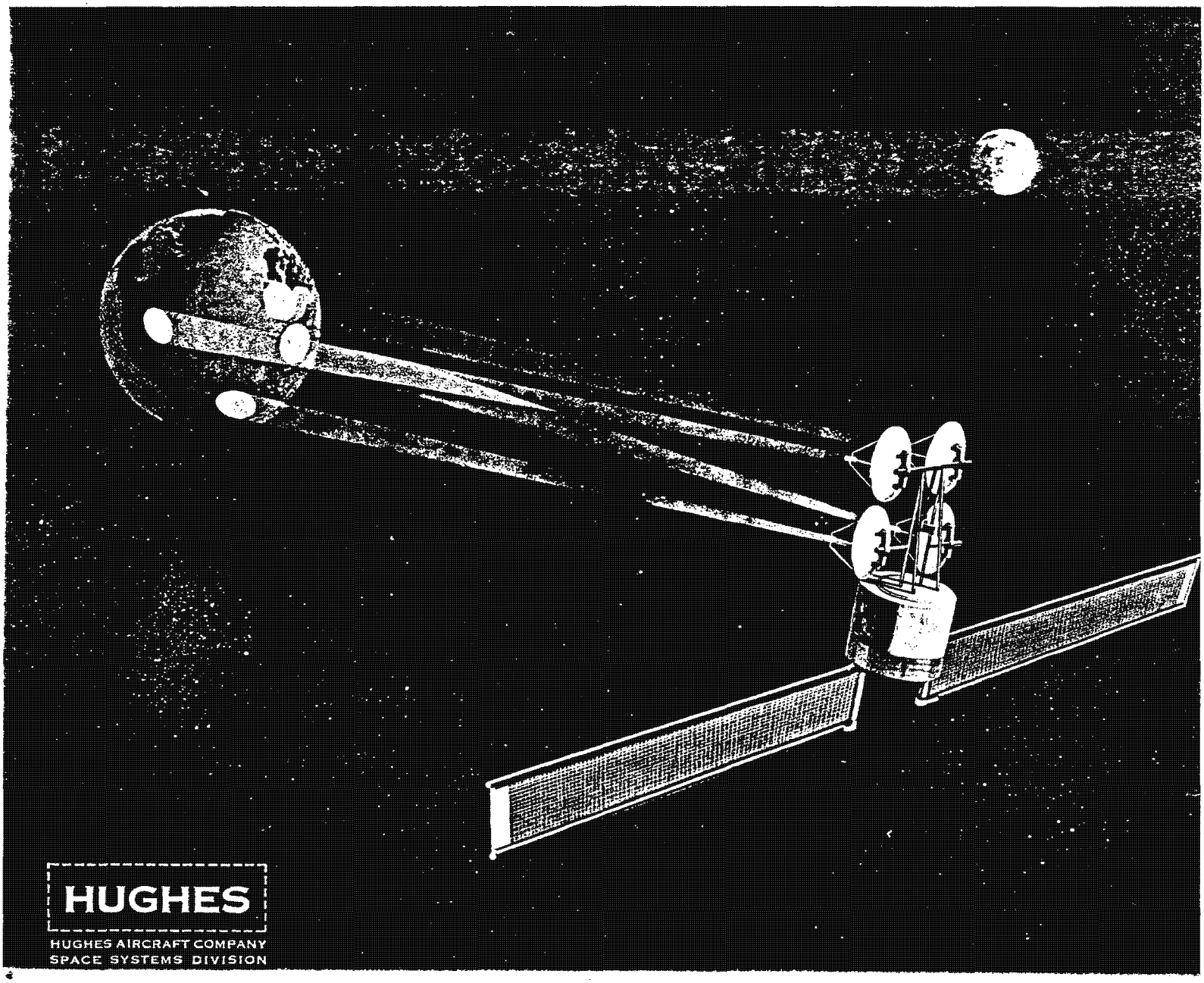

HUGHES

HUGHES AIRCRAFT COMPANY
SPACE SYSTEMS DIVISION

ANALYSES RELATED TO THE HUGHES GYROSTAT SYSTEM

A. J. IORILLO
Assistant Manager
Advanced Design
Satellite Systems Laboratories

HUGHES
HUGHES AIRCRAFT COMPANY
SPACE SYSTEMS DIVISION

DECEMBER 1967

Approved for Release: 2019/01/11 C05105855

PREFACE

This document is a compilation of four papers written during the course of Gyrostat development. The first two comprise analyses which led to formulation of the general nutational stability criterion for dual-spin satellites. The third paper summarizes the subsequent practical application of the theoretical results. The last paper discusses operational and performance aspects of Gyrostat systems.

CONTENTS

	Page
"Nutation Damping" Hughes Aircraft Company IDC 2230. 14/69 October 1964	1-1
"Nutation Damping Dynamics of Rotor Stabilized Satellites" Presented at ASME Annual Winter Meeting Chicago, Illinois November 1965	2-1
"Development of Hughes Gyrostat System" Hughes Aircraft Company SSD 70012R January 1967	3-1
"Precision Aspects of Hughes Gyrostat System" Presented at Dual-Spin Satellite Symposium Aerospace Corporation, Los Angeles, California August 1967	4-1

NUTATION DAMPING

ABSTRACT

A nutational stability criterion is derived for dual-body satellites, such as OSO. The derivation comprises Routh-Hurwitz analysis of linearized system equations and subsequent physical interpretation of the result.

I. INTRODUCTION

The object of the following analysis is a stability criterion which ensures that nutations experienced by a dual-body satellite, such as OSO, will decay when damping is introduced. The criterion sought is analogous to that for a simple spinning body, like Syncom, which states that the body must be spun about its axis of maximum inertia.

The approach taken is somewhat different from that used to establish the single-body criterion. For the single body, kinetic energy considerations, in conjunction with momentum conservation, serve to establish the criterion. Since dual-body satellite momentum and kinetic energy are defined by three quantities (vehicle rate, wheel rate, and nutation angle), the two equations do not suffice to solve for the nutation angle change unless assumptions are made regarding the wheel and vehicle rates. Certainly, sensible assumptions can be made and the criterion may be derived using momentum and energy considerations. However, as in the single-body case, no insight into the mechanics of nutation damping is derivable from an energy dissipation analysis. Thus, the approach taken here is mechanistic. That is, the equations of motion for a dual-body system with a damper are written. Then small oscillations about a steady spin condition are assumed, resulting in a linearized dynamical system. This linear system is examined to determine the stability conditions.

As a result of this approach, a physical description is derived of the reaction torque on the vehicle due to damper action causing nutation damping. The concept of a "roving" dynamic unbalance which causes a resonant damping torque is presented.

The damper considered in the analysis is the mechanical analog of the Syncom mercury-in-a-curved-tube damper at small nutation angles.

II. DISCUSSION

Dual-Body Vehicle

The dual-body configuration considered is shown in Figure 1. Both the wheel and the main satellite are bodies of revolution. The wheel spin axis is coincident with the satellite spin axis. The wheel spin inertia is I_w, the satellite spin inertia is C, and the combined vehicle transverse inertia is A. In an equilibrium steady spin, the vehicle angular momentum is

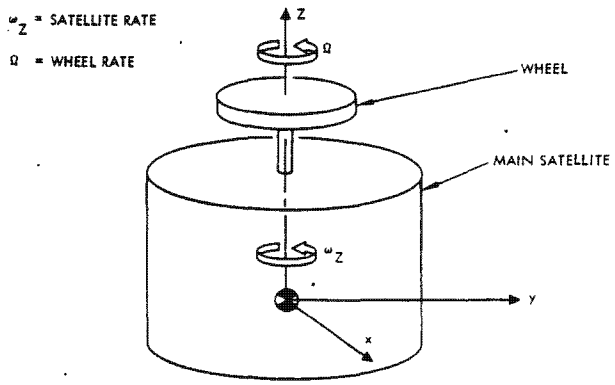

Figure 1. Dual-Body Vehicle

$$C\,\omega_z + I_w\,\Omega$$

Nutation Damper

The nutation damper configuration assumed is shown in Figure 2. The damper consists of a small mass, m, constrained to travel in a tube located on the vehicle x axis. The displacement of the mass is along the body z axis and is denoted by z. The mass is coupled with the body through a spring and linear damper with constants k and c, respectively. The mass of the vehicle is M, and

$$M >>> m$$

The spacecraft transverse inertia is A when the damper is at z = 0.

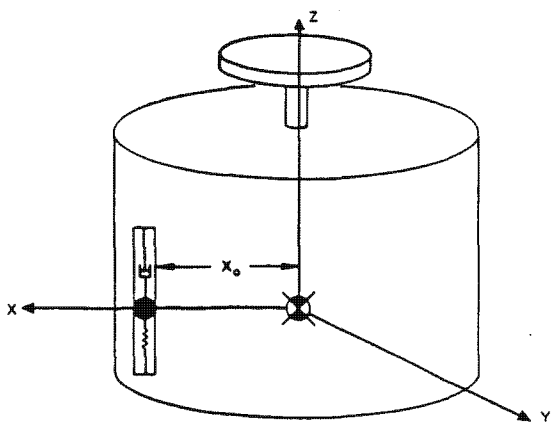

Figure 2. Nutation Damper

III. EQUATIONS OF MOTION

The x, y, z system shown in Figure 1 has its origin at the system mass center and is fixed in the main satellite. The rotation of the x, y, z system is

$$\bar{\omega} = \omega_x\, i + \omega_y\, j + \omega_z\, k$$

~ i, j, k = unit vectors along xyz

The torque-free equations of motion for the vehicle-damper system are:

$$(A+mz^2)\dot{\omega}_x + (C-A-mz^2)\omega_y\omega_z + I_w\Omega\omega_y = mx_o\, z\, \dot{\omega}_z$$

$$+ mx_o\, z\, \omega_x\omega_y - 2m\, z\dot{z}\, \omega_x$$

$$(A+mz^2)\dot{\omega}_y - (C-A-mz^2)\omega_x\omega_z - I_w\Omega\omega_x = mx_o\, \ddot{z}$$

$$- mx_o\, z\left(\omega_x^2 - \omega_z^2\right) - 2m\, z\dot{z}\, \omega_y$$

$$C\dot{\omega}_z = m\, x_o\, z\, \dot{\omega}_x - m\, x_o\, z\, \omega_y\omega_z + 2\, m\, x_o\, \dot{z}\, \omega_x + T_f$$

$$I_w\dot{\Omega} = -T_f$$

$$m\ddot{z} + c\dot{z} + kz = m\, x_o\, \dot{\omega}_y - m\, x_o\, \omega_x\omega_z$$

$$+ m\, z\left(\omega_x^2 + \omega_y^2\right) \qquad (1)$$

where

T_f = frictional bearing torque between wheel and satellite

$\frac{m}{M} \ll 1$

In a steady spin condition,

$$\omega_x = \omega_y = z = 0$$

$$C\dot{\omega}_z + I_w\dot{\Omega} = 0$$

Now consider a very slight deviation from the steady spin condition, a small nutation angle. Then quantities ω_x, ω_y, and z and their rates of change are accordingly very small.

Neglecting products of small quantities, the torque-free equations of motion given above become:

$$A\dot{\omega}_x + (C-A)\omega_z\omega_y + I_w\Omega\omega_y = mx_o\, z\, \dot{\omega}_z$$

$$A\dot{\omega}_y - (C-A)\omega_z\omega_x - I_w\Omega\omega_x = mx_o\cdot\ddot{z} + mx_o\omega_z^2\cdot z$$

$$C\dot{\omega}_z = T_f$$

$$I_w\dot{\Omega} = -T_f$$

$$m\ddot{z} + c\dot{z} + kz = mx_o\dot{\omega}_y - mx_o\omega_z\cdot\omega_x \qquad (2)$$

Equation 2 describes the system motion for small wobbles. Now assume that the friction torque, T_f, is small such that the change in vehicle and wheel rates are very small during the wobble period. This is a sensible assumption since the wheel used should be essentially frictionless. Then,

$$A\omega_x + \left\{(C-A)\omega_z + I_w\Omega\right\}\omega_y = 0$$

$$A\omega_y - \left\{(C-A)\omega_z + I_w\Omega\right\}\omega_x = mx_o\cdot\ddot{z} + mx_o\omega_z^2\cdot z$$

$$\ddot{z} + \frac{c}{m}\dot{z} + \frac{k}{m}z = x_o\dot{\omega}_y - x_o\omega_z\cdot\omega_x \qquad (3)$$

Defining

$$\lambda = \frac{(C-A)\omega_z + I_w\Omega}{A}$$

$$\beta = \frac{c}{m}$$

$$\omega_1 = \sqrt{\frac{k}{m}} = \text{damper natural frequency}$$

Then,

$$\dot{\omega}_x + \lambda\omega_y = 0$$

$$\dot{\omega}_y - \lambda\omega_x = \left(\frac{m\,x_o}{A}\right)\ddot{z} + \left(\frac{m\,x_o}{A}\right)\omega_z^2\, z$$

$$\ddot{z} + \beta\dot{z} + \omega_1^2\, z = x_o\dot{\omega}_y - x_o\omega_z\cdot\omega_x \qquad (4)$$

where the quantity λ is the system nutation frequency. It is noted that the relations in Equation 3 are identical to those describing a single spinning body characterized by a nutation frequency λ. The presence of a wheel merely changes the nutation frequency. Therefore, what follows is valid for the single-body case.

Equation 3 forms a linear system and may be analyzed by standard methods. The system characteristic equation is

$$\left(1 - \frac{mx_o^2}{A}\right)S^4 + \beta S^3 + \left(\omega_1^2 + \lambda^2 - \frac{mx_o^2}{A}\left(\omega_z\lambda + \omega_z^2\right)\right)S^2$$

$$+ \beta\lambda^2 S + \omega_1^2\lambda^2 - \frac{mx_o^2}{A}\lambda\omega_z^3$$

A Routh-Hurwitz analysis indicates that stability requires

$$1)\quad \frac{mx_o^2}{A}\left(\lambda^2 - \lambda\omega_z - \omega_z^2\right) + \omega_1^2 > 0$$

2) $\lambda \left(\lambda \omega_1^2 - \frac{mx_o^2}{A} \omega_z^3 \right) > 0$

3) $\lambda \left(\lambda - \omega_z \right) \left(\lambda^2 - \omega_z^2 \right) > 0$

when

$$\frac{mx_o^2}{A} \to 0$$

The meaningful condition (3 above) is

$$\lambda \left(\lambda - \omega_z \right) \left(\lambda^2 - \omega_z^2 \right) > 0$$

Condition 3 may be rewritten as

$$\lambda \left(\lambda + \omega_z \right) \left(\lambda - \omega_z \right)^2 > 0$$

Then the condition is

$$\lambda \left(\lambda + \omega_z \right) > 0$$

By defining the initial spin momentum as a positive quantity, the stability condition becomes

$$\boxed{\lambda > 0}$$

As expected, this condition is the same as the result for a single spinning body. Although this form is much simpler, condition 3 has physical significance, as shown later in this paper.

IV. PHYSICAL INTERPRETATION OF RESULT

Consider the equation of motion for the damper mass:

$$\ddot{z} + \beta \dot{z} + \omega_1^2 z = x_o \dot{\omega}_y - (x_o \omega_z) \omega_x \qquad (5)$$

The transverse rates ω_x and ω_y are forcing functions for damper motion. Consider a freely nutating body before damping is effective. Then,

$$\omega_x = \omega_o \cos \lambda t$$

$$\omega_y = \omega_o \sin \lambda t$$

Substituting into Equation 5 yields

$$\ddot{z} + \beta \dot{z} + \omega_1^2 z = x_o \omega_o (\lambda - \omega_z) \cos \lambda t$$

This is the familiar equation of a damped harmonic oscillator, sinusoidally forced. The forced response is

$$z(t) = \frac{x_o \omega_o (\lambda - \omega_z)}{\left(\omega_1^2 - \lambda^2 \right)^2 + \left(\beta \lambda \right)^2} \left[\beta \lambda \sin \lambda t + \left(\omega_1^2 - \lambda^2 \right) \cos \lambda t \right]$$

The effect of the damper mass motion on the satellite is given by

$$\dot{\omega}_x + \lambda \omega_y = 0$$

$$\dot{\omega}_y - \lambda \omega_x = \left(\frac{mx_o}{A} \right) \omega_z^2 z + \left(\frac{mx_o}{A} \right) \ddot{z} \qquad (6)$$

The term

$$\frac{mx_o}{A} z \cdot \omega_z^2$$

is recognized as a "dynamic unbalance" term. The term

$$\frac{mx_o}{A} \ddot{z}$$

represents the torque due to the reaction force of the restraining spring and damper. Substituting z(t) into Equation 6 results in

$$\dot{\omega}_x + \lambda \omega_y = 0$$

$$\dot{\omega}_y - \lambda \omega_x = -\frac{mx_o^2}{A} \omega_o \beta \frac{\lambda \left(\lambda - \omega_z \right) \left(\lambda^2 - \omega_z^2 \right)}{\left(\omega_1^2 - \lambda^2 \right)^2 + \left(\beta \lambda \right)^2} \sin \lambda t$$

$$- \frac{mx_o^2}{A} \omega_o \frac{\left(\lambda - \omega_z \right) \left(\lambda^2 - \omega_z^2 \right) \left(\omega_1^2 - \lambda^2 \right)}{\left(\omega_1^2 - \lambda^2 \right)^2 + \left(\beta \lambda \right)^2} \cos \lambda t \qquad (7)$$

Equation 7 is seen to be of the form

$$\dot{\omega}_x + \lambda \omega_y = 0$$

$$\dot{\omega}_y - \lambda \omega_x = A \omega_y + B \omega_x$$

The term $A \omega_y$ is a "damping" term. The sign of the damping constant A is governed by

$$\lambda \left(\lambda - \omega_z \right) \left(\lambda^2 - \omega_z^2 \right)$$

the same criterion obtained earlier. The term $B \omega_x$ represents a torque normal to the rotating transverse angular velocity vector tending to "turn" the vector rather than affecting its magnitude. These concepts are explained later.

Now, to solve Equation 7, it may be rewritten as

$$\dot{\omega}_x + \lambda \omega_y = 0$$

$$\dot{\omega}_y - \lambda \omega_x = -\frac{mx_o^2}{A}\,\omega_o \frac{(\lambda - \omega_z)(\lambda^2 - \omega_z^2)}{\sqrt{(\lambda^2 - \omega_1^2)^2 + (\beta\lambda)^2}} \cos(\lambda t - \psi_1) \tag{8}$$

where

$$\psi = \tan^{-1} \frac{\beta\lambda}{\omega_1^2 - \lambda^2}$$

Equation 8 may be solved in quadrature. Letting

$$M_y = -\frac{mx_o^2}{A}\omega_o \cdot \frac{(\lambda - \omega_z)(\lambda^2 - \omega_z^2)}{\sqrt{(\lambda_2 - \omega_1^2)^2 + (\beta\lambda)^2}}$$

$$\cos(\lambda t - \psi) = \frac{e^{-i\psi}}{2} \cdot e^{i\lambda t} + \frac{e^{i\psi}}{2} \cdot e^{-i\lambda t}$$

$$\omega = \omega_x + i\,\omega_y, \quad i = \sqrt{-1}$$

the solution is

$$\omega(t) = \left[\omega_o + i\frac{M_y}{2} e^{-i\psi} \cdot t\right] e^{i\lambda t} + \frac{M_y}{2\lambda} e^{i\psi} \sin \lambda t \tag{9}$$

The nutation angle history is given by

$$\theta(t) \cong \frac{A}{C\,\omega_z} \cdot |\omega(t)|$$

Equation 9 reveals several interesting results. The effect of damper motion at nutation frequency, causing a resonant torque which acts in a constant fashion on the initial rate ω_o, and the effect of "tuning" the damper are observable. For a tuned damper,

$$\omega_1 = \sqrt{\frac{k}{m}} = \lambda$$

$$\psi = \pi/2$$

The decay term becomes

$$\theta(t) = \frac{A\omega_o}{C\omega_z}\left\{1 - \frac{mx_o^2}{A}\,\frac{\lambda(\lambda - \omega_z)(\lambda^2 - \omega_z^2)}{2\beta\lambda^2}\,t\right\}$$

Thus, tuning the damper places the damping moment along the initial angular velocity vector thereby maximizing its effectiveness.

Using these results, a physical picture of the damping process may be constructed. The rotation of the angular velocity vector relative to the body gives rise to inertial forces driving the damper mass up and down. The mass then becomes a roving dynamic unbalance with frequency λ. However, due to damping, β, the mass lags the transverse velocity vector. Since the reaction moment due to mass motion is along an axis normal to the damper plane, the lag places a component of the reaction moment along the transverse angular velocity. Further, since the reaction moment frequency is resonant with the transverse rate, the reaction moment acts constantly to either increase or decrease the angular rate. If the phase lag is 90 degrees, the total reaction moment acts along the transverse angular velocity.

From the representation of the damper reaction moment as a vector rotating in body coordinates, it was seen that the moment is the sum of two counterrotating vectors

$$\sim \frac{e^{-i\psi}}{2} e^{i\lambda t} + \frac{e^{i\psi}}{2} e^{-i\lambda t}$$

This is the result of having a single damper. If there were two dampers spaced 90 degrees apart, the reaction moment could be represented by a single vector rotating at nutation frequency

$$M(t) \sim e^{i\lambda t}$$

To fix ideas, consider Figure 3. The damping mass has displaced from its equilibrium location in its attempt to get as far from the total angular velocity vector $\bar{\omega}$ as possible. The reaction forces on the body cause the moment $\bar{M}$ along the y axis. When the vector $\bar{\omega}$ rotates through 180 degrees, the mass tends to move as indicated.

The resultant reaction moment now acts along the negative y axis. Due to damping, β, the mass motion lags $\bar{\omega}$. For simplicity of illustration, consider the two-damper case. Here, the moment $\bar{M}$ can be considered a rotating vector. Then the concept of the lag can be thought of as shown in Figure 4a. The vectors $\bar{\omega}$ and $\bar{M}$ rotate at the same frequency, allowing the damping component to act continuously along the vector ω. For the case of $\lambda < 0$, the unstable condition, the same moment $\bar{M}$ would be located relative to $\bar{\omega}$ as shown in Figure 4b. Here, the component of $\bar{M}$ along $\bar{\omega}$ acts to increase $\bar{\omega}$ and thus increases the nutation angle. The validity of these representations may be checked by considering the detailed motion of the mass and the resultant moment for the two cases $\lambda > 0$ and $\lambda < 0$. The principal difference between the two cases is the rotational sense of the transverse angular velocity vector relative to the spin sense. The lag, in the stable case, tips the moment $\bar{M}$ away from the vector $\bar{\omega}$. For the unstable case, the vector $\bar{M}$ is tipped into the vector $\bar{\omega}$.

Although a specific damper was selected for the analysis, the same concepts may be extended. The induced relative motion at

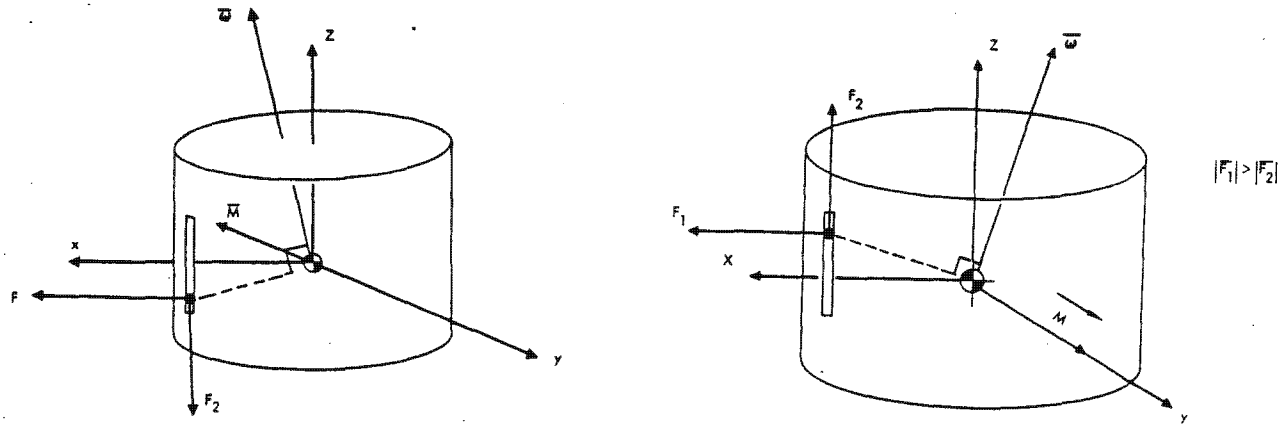

Figure 3. Damper Mass Dynamics

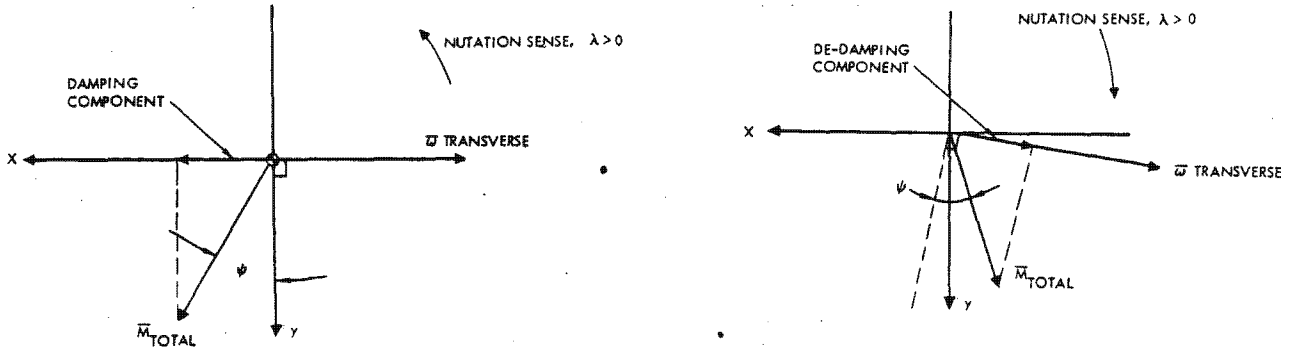

a) Stable Case

b) Unstable Case

Figure 4. Lag Concept

nutation frequency, the resultant roving dynamic unbalance, the lag caused by damping, and the relative orientation of the moment and the transverse angular velocity vector may be extended to the quasi-rigid body where the body itself experiences a cyclic distortion of its inertial symmetry giving rise to dynamic unbalance.

Further detailed study of the mass motion unveils the second-order reaction torque acting along the spin axis. This torque causes a change in spin rate required to conserve momentum. This reaction torque is due to a coriolis reaction between the mass and the body. The direction of this torque is also dependent on the nutation sense.

V. CONCLUDING REMARKS

The dual body (as the single body) must satisfy the condition

$$\boxed{\lambda > 0}$$

relative to the body carrying the nutation damper to ensure stability.

Thus, when a despun section is added to Syncom, the configuration must be designed such that

$$\frac{C}{A} > 1$$

NUTATION DAMPING DYNAMICS OF AXISYMMETRIC ROTOR STABILIZED SATELLITES

ABSTRACT

The equations of motion of a dual-body configuration with nutation dampers in each body are linearized about an initial nutation angle. The linear equations are then solved, yielding the relation between system parameters and nutation angle change. The solutions are compared to those obtained by applying energy principles and are found to be identical. Further, from the dynamic analysis, insight is derived into the operation of pendulous nutation dampers. It is shown that nutational stability of dual-spin systems can be achieved for nearly any system inertial distribution.

NOMENCLATURE

C = moment of inertia about configuration figure axis of body I (with damper mass at rest)

I = moment of inertia about configuration figure axis of body II (with damper mass at rest)

A = transverse moment of inertia of entire configuration (with damper masses at rest)

Ω_I = spin rate of body I

Ω_{II} = spin rate of body II

ω_o = initial transverse angular rate of entire configuration

$$\lambda_o = \frac{C\Omega_I + I\Omega_{II}}{A}$$

$$\lambda_I = \lambda_o - \Omega_I$$

$$\lambda_{II} = \lambda_o - \Omega_{II}$$

$\dot{T}_I$ = energy dissipation rate in body I

$\dot{T}_{II}$ = energy dissipation rate in body II

J = motor torque

ω_x = configuration angular rate about 0X

ω_y = configuration angular rate about 0Y

ω'_x = perturbation angular rate about 0X

ω'_y = perturbation angular rate about 0Y

m_I, m_{II} = damper masses in bodies I and II

c_I, c_{II} = oscillator damping constants

k_I, k_{II} = oscillator spring constants

$$\beta_I, \beta_{II} = \frac{c_I}{m_I}, \frac{c_{II}}{m_{II}}$$

$$\omega_I^2 = \frac{k_I}{m_I} - \omega_o^2$$

$$\omega_{II}^2 = \frac{k_{II}}{m_{II}} - \Omega_{II}^2 - \frac{\omega_o^2}{2}$$

X_o = distance from 0Z of oscillator in body I

h_o = distance from 0XY of oscillator in body II

$z(t)$ = displacement of damper mass, m_I

$\rho(t)$ = displacement of damper mass, m_{II}

$\varphi_I = \int \Omega_I \, dt$

$\varphi_{II} = \int \Omega_{II} \, dt$

I. INTRODUCTION

This paper discusses passive damping of the transient motion, nutation, of dual-body satellite configurations typified by the OSO I satellite which is composed of two bodies free to rotate relative to each other.

Recent works (References 1 and 2) derive nutational stability criteria for dual-body configurations by applying energy and momentum principles similar to the approach taken by Thomson and Reiter (Reference 3) in deriving the criterion for spin-stabilized satellites. However, each of these works considers only the special case of configurations where one of the bodies is rigid. They find that a vehicle stabilized by a rigid rotor is essentially free of inertia constraints and that a rigid platform stabilized by a nonrigid rotor is subject to the classical inertia constraints, i.e., the rotor spin inertia must be larger than vehicle transverse inertias.

Here, the general case of dual-body vehicles with dissipation in both bodies is considered. An energy analysis is performed, and general criteria are derived. To illustrate the tacit assumptions made in the analysis and to corroborate the results, the equations of motion of a

dual-body configuration with energy dissipators in each body are solved. The angular velocity changes predicted by the two analyses are compared and shown to be identical. The general criteria indicate that all dual-body configurations can be made stable by adjusting the energy dissipation rates on each body. (The practical implication is that platforms stabilized by nonrigid rotors which violate the earlier criterion can be made stable simply by placing an efficient nutation damper on the platform.)

II. ENERGY-MOMENTUM CONSIDERATIONS

A dual-body configuration is illustrated in Figure 1. Except for rotation about the axis of symmetry, bodies I and II are rigidly joined. For convenience, and without loss of generality, ω and λ_o are defined as always positive. Thus the nutation angle, θ, is understood to be measured from the direction of the positive angular momentum vector, as shown in Figure 1. Consider the case when the bodies are uncoupled in spin and free of exterior torques. The system angular momentum, h_o, and kinetic energy, T, are

$$h_o^2 = (C\Omega_I + I\Omega_{II})^2 + (A\omega)^2 \qquad (1)$$

$$2T = A\omega^2 + C\Omega_I^2 + I\Omega_{II}^2 \qquad (2)$$

To investigate the change in angular rates when energy is dissipated in the system, the derivatives of Equations 1 and 2 are combined, resulting in

$$\dot{T} = \dot{T}_I + \dot{T}_{II} = -C\lambda_I\dot{\Omega}_I - I\lambda_{II}\dot{\Omega}_{II} \qquad (3)$$

where $\dot{T}$ is the rate at which "work" is done by nonconservative forces within the system. In this sense, it is the rate at which energy is dissipated. Since it is assumed that both bodies contain dissipative mechanisms, the total rate is written as the sum of the dissipation rates in each body, $\dot{T}_I$ and $\dot{T}_{II}$. As such, both quantities are always negative.

Since the bodies are assumed uncoupled, it is possible to identify the reaction torques acting on the bodies tending to change the rates:

$$C\dot{\Omega}_I = -\frac{\dot{T}_I}{\lambda_I}, \quad I\dot{\Omega}_{II} = -\frac{\dot{T}_{II}}{\lambda_{II}} \qquad (4)$$

$$A\omega\dot{\omega} = \lambda_o\left(\frac{\dot{T}_I}{\lambda_I} + \frac{\dot{T}_{II}}{\lambda_{II}}\right) \qquad (5)$$

The energy dissipation implicit in the analysis is a consequence of the motion of nonrigid elements within the system. It is assumed that

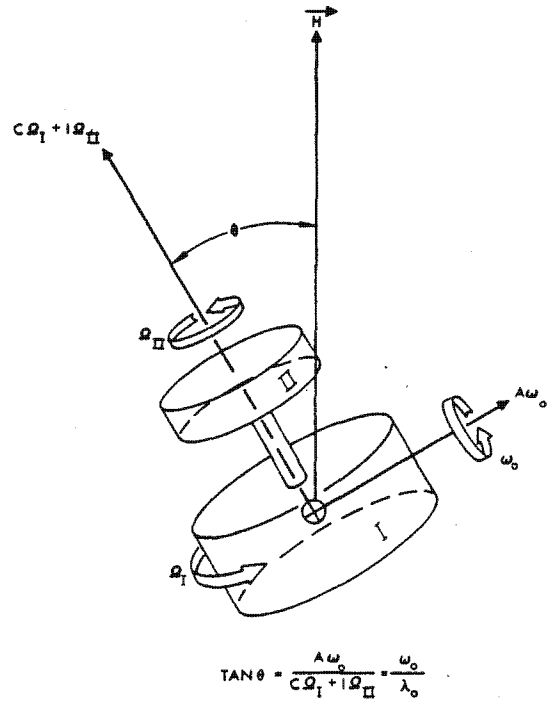

Figure 1. Dual-Body Configuration

the energy and momentum associated with internal motion, and deviations of system inertias from steady-state values, are negligible. Since no dissipation is allocated to damping of transient relative motion of internal elements, the analysis does not presume to apply to situations wherein transients are important. During nutation, sustained relative motion is possible by virtue of cyclic body forces acting throughout the bodies. The fundamental frequencies of these cyclic inertial forces are λ_I and λ_{II}, the nutation frequencies with respect to the bodies. Should λ_I or λ_{II} be zero, the inertial forces in that body are static, and internal motion (thus, energy dissipation) cannot persist in the presence of damping.

Proceeding with the analysis, the system is stable, $\dot{\omega} < 0$, when

$$\lambda_I,\ \lambda_{II} > 0$$

$$\lambda_I > 0,\ \lambda_{II} < 0 \text{ and } \left|\frac{\dot{T}_I}{\lambda_I}\right| > \left|\frac{\dot{T}_{II}}{\lambda_{II}}\right| \qquad (6)$$

$$\lambda_I < 0,\ \lambda_{II} > 0 \text{ and } \left|\frac{\dot{T}_I}{\lambda_I}\right| < \left|\frac{\dot{T}_{II}}{\lambda_{II}}\right|$$

As indicated by Equation 4, the secular transverse rate change must be accompanied by secular spin rate changes. If the conditions in Equation 6 are satisfied, the nutation angle, θ, will decrease since

$$\tan \theta = \frac{\omega}{\lambda_o}$$

However, as ω decreases, the body spin rates, and hence nutation frequencies, change. If the nutation frequency in one of the bodies, say I, diminishes to zero before $\theta = 0$ is reached, the energy dissipation, $\dot{T}_I$, ceases and that body acts like a rigid body. If body II were rigid, the system would be content to remain at this terminal nutation angle. This result is easily visualized by considering the space-viewed motion of body I when

$$\lambda_o = \Omega_I \neq 0$$

In this state, each element in I rotates steadily about the space-fixed angular momentum vector at the rate λ_o. The body forces in I are then static. The forces in II are clearly cyclic, but since that body is assumed rigid, no energy is dissipated in the system. Thus, the configuration should be designed to ensure that, as nutations are damped, the nutation frequency with respect to the body containing the primary energy dissipation mechanism does not vanish. (This is the essence of the discussion of stability regions presented in Reference 1.)

To consider the effect of a motor torque, J, coupling the bodies, Equation 3 is written

$$\dot{T} = \dot{T}_I + \dot{T}_{II} = A\omega\dot{\omega} + (C\dot{\Omega}_I + J)\Omega_I + (I\dot{\Omega}_{II} - J)\Omega_{II} \qquad (7)$$

The stability criteria may be derived for this case by assuming one of the bodies is rigid. The result of this assumption, assuming body II to be rigid, is

$$\lambda_I > 0$$

as found in Equation 1. Alternately, it may be assumed that the torque is applied to keep one of the bodies at a constant rate, say body I, such that

$$I\dot{\Omega}_{II} + \frac{\dot{T}_{II}}{\lambda_{II}} + \frac{\dot{T}_{II}}{\lambda_I} = 0$$

and

$$A\omega\dot{\omega} = \lambda_o\left(\frac{\dot{T}_I}{\lambda_I} + \frac{\dot{T}_{II}}{\lambda_{II}}\right)$$

duplicating Equation 5. Thus, for two practical cases of interest, the stability criteria may be inferred from the conditions given in Equation 6. Although the criteria are not affected by the torque, the motor can change the momentum distribution between the bodies and thereby change the nutation frequencies seen by them.

From the preceding results, it is seen that a dual-spin system of nearly any inertial configuration can be rendered nutationally stable by proper adjustment of energy dissipation rates.

III. DYNAMIC ANALYSIS

To corroborate the foregoing arguments and to demonstrate, by example, the underlying assumptions of the energy analysis, the motion of a dual-body satellite with nutation dampers in each body is studied. The nutation dampers are assumed to be simple damped harmonic oscillators. However, they are analogous in principle to pendulum dampers currently used in Syncom and OSO I, and help develop insight into the mechanics of "real" dampers.

System Equations of Motion

The dual-body configuration to be analyzed is illustrated in Figure 2. Each body contains an energy dissipation mechanism, idealized as a single-degree-of-freedom damped harmonic oscillator. The oscillator in body I is oriented parallel to the OZ axis and located a distance x_o from the axis. When the oscillator is at rest, the mass, m_I, lies in the transverse plane containing the configuration center of mass. The oscillator in body II is oriented normal to the OZ axis at $z = h_o$. When the mass, m_{II}, is at rest, it lies on the OZ axis. It is assumed that the oscillator masses are small relative to the system mass, so that the center of mass is essentially stationary

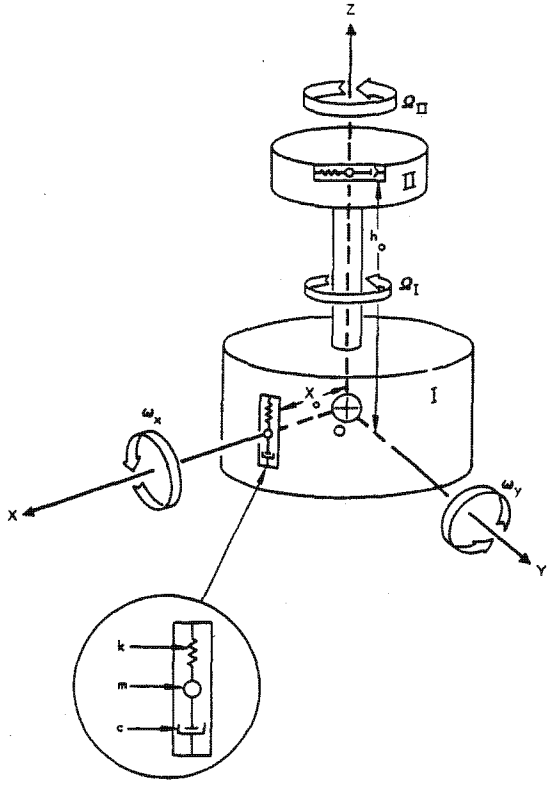

Figure 2. Reference Frame and Nutation Damper Geometry

in body coordinates. The system equations of motion relative to the OXYZ frame, with origin at the center of mass and nonspinning, are then

$$A\dot{\omega}_x + \{C\Omega_I + I\Omega_{II}\}\omega_y + m_I z^2 \dot{\omega}_x + 2m_I z\dot{z}\omega_x$$

$$+ m_I x_o z(-\omega_y^2 \sin\varphi_I - \omega_x\omega_y \cos\varphi_I)$$

$$+ m_I x_o \ddot{z} \sin\varphi_I - m_I x_o z(\dot{\Omega}_I \cos\varphi_I - \Omega_I^2 \sin\varphi_I)$$

$$+ m_{II}\rho^2(\dot{\omega}_x \sin^2\varphi_{II} - \dot{\omega}_y \sin\varphi_{II}\cos\varphi_{II})$$

$$- m_{II} h_o \rho(\omega_y^2 \sin\varphi_{II} + \omega_x\omega_y \cos\varphi_{II})$$

$$- m_{II}h_o(\ddot{\rho} - \rho\Omega_{II}^2)\sin\varphi_{II} - m_{II}h_o(2\dot{\rho}\Omega_{II} + \rho\dot{\Omega}_{II})\cos\varphi_{II}$$

$$+ m_{II}[2\rho\dot{\rho}\sin^2\varphi_{II} + 2\rho^2\Omega_{II}\sin\varphi_{II}\cos\varphi_{II}]\omega_x$$

$$- m_{II}[2\rho\dot{\rho}\sin\varphi_{II}\cos\varphi_{II} - 2\rho^2\Omega_{II}\sin^2\varphi_{II}]\omega_y = 0$$

$$A\dot{\omega}_y - \{C\Omega_I + I\Omega_{II}\}\omega_x + m_I z^2\dot{\omega}_y + 2m_I z\dot{z}\omega_y$$

$$+ m_I x_o z[\omega_x^2 \cos\varphi_I + \omega_x\omega_y \sin\varphi_I]$$

$$- m_I x_o \ddot{z}\cos\varphi_I - m_I x_o z(\dot{\Omega}_I \sin\varphi_I + \Omega_I^2\cos\varphi_I)$$

$$- m_{II}\rho^2[\dot{\omega}_x \sin\varphi_{II}\cos\varphi_{II} - \dot{\omega}_y\cos^2\varphi_{II}]$$

$$+ m_{II}h_o\rho[\omega_x^2\cos\varphi_{II} + \omega_x\omega_y\sin\varphi_{II}]$$

$$+ m_{II}h_o(\ddot{\rho} - \rho\Omega_{II}^2)\cos\varphi_{II} - m h_o(2\dot{\rho}\Omega_{II} + \rho\dot{\Omega}_{II})\sin\varphi_{II}$$

$$+ m_{II}[2\rho\dot{\rho}\cos^2\varphi_{II} - 2\rho^2\Omega_{II}\sin\varphi_{II}\cos\varphi_{II}]\omega_y$$

$$- m_{II}[2\rho\dot{\rho}\sin\varphi_{II}\cos\varphi_{II} + 2\rho^2\Omega_{II}\cos^2\varphi_{II}]\omega_x = 0$$

$$C\dot{\Omega}_I - m_I x_o z(\dot{\omega}_x\cos\varphi_I + \dot{\omega}_y\sin\varphi_I)$$

$$- 2m_I x_o \dot{z}(\omega_x\cos\varphi_I + \omega_y\sin\varphi_I) + J = 0$$

$$I\dot{\Omega}_{II} - m_{II}h_o\rho(\dot{\omega}_x\cos\varphi_{II} + \dot{\omega}_y\sin\varphi_{II})$$

$$+ 2m_{II}\rho\dot{\rho}\Omega_{II} + m_{II}\rho^2\dot{\Omega}_{II} + m_{II}\rho^2[\omega_x\omega_y(\cos^2\varphi_{II}$$

$$- \sin^2\varphi_{II}) + (\omega_y^2 - \omega_x^2)\sin\varphi_{II}\cos\varphi_{II}] - J = 0 \qquad (8)$$

The complementary equations of motion for the oscillator masses are

$$\ddot{z} + \frac{c_I}{m_I}\dot{z} + \frac{k_I}{m_I}z + x_o(\dot{\omega}_x\sin\varphi_I - \dot{\omega}_y\cos\varphi_I)$$

$$- z(\omega_x^2 + \omega_y^2) + 2x_o\Omega_I(\omega_x\cos\varphi_I + \omega_y\sin\varphi_I) = 0$$

$$\ddot{\rho} + \frac{c_{II}}{m_{II}}\dot{\rho} + \frac{k_{II}}{m_{II}}\rho - h_o(\dot{\omega}_x\sin\varphi_{II} - \dot{\omega}_y\cos\varphi_{II})$$

$$- \rho\Omega_{II}^2 - \rho\omega_y^2\cos^2\varphi_{II} - \rho\omega_x^2\sin^2\varphi_{II}$$

$$+ 2\rho\omega_x\omega_y\sin\varphi_{II}\cos\varphi_{II} = 0 \qquad (9)$$

Equations 8 and 9 are the complete system equations of motion, recalling the assumption that m_I and m_{II} are very small relative to the total system mass.

Linearization About Initial Nutation

If the dampers were caged, Equation 8 reduces to the ordinary Euler equations written with respect to a nonrotating body-fixed frame. The nutational motion of the configuration in this state is described by

$$\omega_x(t) = \omega_o \cos\lambda_o t$$

$$\omega_y(t) = \omega_o \sin\lambda_o t$$

To examine the effect of oscillator motion, the following assumptions are made. The oscillator springs are stiff enough to prevent "bottoming" of the masses or

$$\frac{k_I}{m_I} > \omega_o^2 \quad , \quad \frac{k_{II}}{m_{II}} > \omega_o^2 + \Omega_{II}^2$$

and the damping forces are large enough to ensure that ρ and z are small quantities. Further, the time constants associated with secular changes of the vehicle rates are large compared to oscillator damping time constants, permitting neglect of oscillator transients. Moreover, the torque J is applied to keep one of the bodies at a constant rate and not to radically change the spin momentum distribution between the bodies. Introducing:

$$\omega_x(t) = \omega_o \cos\lambda_o t + \omega_x'$$

$$\omega_y(t) = \omega_o \sin\lambda_o t + \omega_y' \qquad (10)$$

where ω_x', ω_y' ~ perturbation rates, substituting into Equations 8 and 9, and neglecting the products of small quantities, yields

$$\dot{\omega}_x' + \lambda_o \omega_y' + \left(\frac{m_I x_o}{A}\right) z \Omega_I^2 \sin \Omega_I t$$

$$- \left(\frac{m_I x_o}{A}\right) z \omega_o^2 \cos(\lambda_o - \Omega_I) t \sin \lambda_o t$$

$$+ \left(\frac{m_I x_o}{A}\right) \ddot{z} \sin \Omega_I t - \left(\frac{m_{II} h_o}{A}\right) \rho \omega_o^2 \cos(\lambda_o$$

$$- \Omega_{II}) t \sin \lambda_o t$$

$$- \left(\frac{m_{II} h_o}{A}\right) (\ddot{\rho} - \rho \Omega_{II}^2) \sin \Omega_{II} t$$

$$- \left(\frac{m_{II} h_o}{A}\right) 2 \dot{\rho} \Omega_{II} \cos \Omega_{II} t = 0$$

$$\dot{\omega}_y' - \lambda_o \omega_x' - \left(\frac{m_I x_o}{A}\right) z \Omega_I^2 \cos \Omega_I t$$

$$+ \left(\frac{m_I x_o}{A}\right) z \omega_o^2 \cos(\lambda_o - \Omega_I) t \cos \lambda_o t$$

$$- \left(\frac{m_I x_o}{A}\right) \ddot{z} \cos \Omega_I t$$

$$+ \left(\frac{m_{II} h_o}{A}\right) \rho [\omega_o^2 \cos(\lambda_o - \Omega_{II}) t \cos \lambda_o t$$

$$+ \left(\frac{m_{II} h_o}{A}\right) (\ddot{\rho} - \rho \Omega_{II}^2) \cos \Omega_{II} t$$

$$- \left(\frac{m_{II} h_o}{A}\right) 2 \dot{\rho} \Omega_{II} \sin \Omega_{II} t = 0$$

$$\dot{\Omega}_I + \frac{m_I x_o}{C} z \omega_o \lambda_o \sin(\lambda_o - \Omega_I) t$$

$$- \frac{2 m_I x_o}{C} \dot{z} \omega_o \cos(\lambda_o - \Omega_I) t + \frac{J}{C} = 0 \qquad (11)$$

$$\dot{\Omega}_{II} + \frac{m_{II} h_o}{I} \rho \omega_o \lambda_o \sin(\lambda_o - \Omega_I) t - \frac{J}{I} = 0$$

$$\ddot{z} + \frac{c_I}{m_I} \dot{z} + \left(\frac{k_I}{m_I} - \omega_o^2\right) z = x_o \omega_o (\lambda_o - 2\Omega_I) \cos(\lambda_o - \Omega_I) t$$

$$\ddot{\rho} + \frac{c_{II}}{m_{II}} \dot{\rho} + \left[\frac{k_{II}}{m_{II}} - \Omega_{II}^2 - \omega_o^2 \sin^2(\lambda_o - \Omega_{II}) t\right] \rho$$

$$= -h_o \omega_o \lambda_o \cos(\lambda_o - \Omega_{II}) t$$

It is observed that the spin rate changes no longer appear in the transverse equations and that, consistent with the assumption of small perturbations,

$$\varphi_I \cong \Omega_I t$$

$$\varphi_{II} \cong \Omega_{II} t$$

The equations describing the perturbation spin rate changes are retained since they are of interest. From these equations, it is seen that the torque J serves to transfer the oscillator torques from one body to the other. Thus, to investigate the effect of oscillator motion on the spin rates, the motor torque need not be considered. The effect of perturbation quantities on oscillator motion is also neglected.

Neglecting transients, oscillator motions are given by

$$z(t) = \frac{x_o \omega_o (\lambda_I - \Omega_I)}{[\omega_I^2 - \lambda_I^2]^2 + \beta_I^2 \lambda_I^2} \left[\beta_I \lambda_I \sin \lambda_I t + (\omega_I^2 - \lambda_I^2) \cos \lambda_I t\right] \qquad (12)$$

$$\rho(t) = \frac{-h_o \omega_o \lambda_o}{[\omega_{II}^2 - \lambda_{II}^2]^2 + \beta_{II}^2 \lambda_{II}^2} \left[\beta_{II} \lambda_{II} \sin \lambda_{II} t\right.$$

$$\left. + (\omega_{II}^2 - \lambda_{II}^2) \cos \lambda_{II} t\right]$$

To facilitate solving for the perturbation transverse rates, let

$$\omega' = \omega_x' + i \omega_y' \qquad (i^2 = 1)$$

and add the first two relations of Equation 11 in quadrature:

$$\frac{d}{dt}\left(\omega' e^{-i\lambda_o t}\right)$$

$$= \left(\frac{m_I x_o}{A}\right)\left[z\Omega_I^2 + \ddot{z}\right] i e^{-i\lambda_I t} - i\left(\frac{m_I x_o}{A}\right)\omega_o^2 z \cos\lambda_I t$$

$$- \left(\frac{m_{II} h_o}{A}\right)\left[\ddot{\rho} - \rho\Omega_{II}^2\right] i e^{-i\lambda_{II} t}$$

$$+ 2\left(\frac{m_{II} h_o}{A}\right)\dot{\rho}\Omega_{II} e^{-i\lambda_{II} t}$$

$$- i\left(\frac{m_{II} h_o}{A}\right)\rho\omega_o^2 \cos\lambda_{II} t \qquad (13)$$

Solution of Linearized Equations

Substituting Equation 12 into 13, integrating and retaining only secular terms gives

$$\omega'(t) = -\left(\frac{m_I x_o^2}{A}\right)\frac{\omega_o(\lambda_I - \Omega_I)(\lambda_I^2 - \Omega_I^2)}{\left[\omega_I^2 - \lambda_I^2\right]^2 + \beta_I^2\lambda_I^2}\left[\beta_I\lambda_I + i(\omega_I^2 - \lambda_I^2)\right]\left(\frac{t}{2}\right) e^{i\lambda_o t}$$

$$- \left(\frac{m_I x_o^2}{A}\right)\frac{(\lambda_I - \Omega_I)\omega_o^3}{\left[\omega_I^2 - \lambda_I^2\right]^2 + \beta_I^2\lambda_I^2}\left[i(\omega_I^2 - \lambda_I^2)\right]\cdot\left(\frac{t}{2}\right)$$

$$\cdot e^{i\lambda_o t} - \left(\frac{m_{II} h_o^2}{A}\right)\frac{\omega_o\lambda_o(\lambda_{II}^2 + \Omega_{II}^2)}{\left[\omega_{II}^2 - \lambda_{II}^2\right]^2 + \beta_{II}^2\lambda_{II}^2}\left[\beta_{II}\lambda_{II} + i(\omega_{II}^2 - \lambda_{II}^2)\right]\cdot\left(\frac{t}{2}\right)\cdot e^{i\lambda_o t}$$

$$- \left(\frac{m_{II} h_o^2}{A}\right)\frac{2\omega_o\lambda_o\Omega_{II}\lambda_{II}}{\left[\omega_{II}^2 - \lambda_{II}^2\right]^2 + \beta_{II}^2\lambda_{II}^2}\left[\beta_{II}\lambda_{II} + i(\omega_{II}^2 - \lambda_{II}^2)\right]\cdot\left(\frac{t}{2}\right) e^{i\lambda_o t}$$

$$+ \left(\frac{m_{II} h_o^2}{A}\right)\frac{\lambda_o\omega_o^3}{\left[\omega_{II}^2 - \lambda_{II}^2\right]^2 + \beta_{II}^2\lambda_{II}^2}\left[i(\omega_{II}^2 - \lambda_{II}^2)\right]\cdot\left(\frac{t}{2}\right)\cdot e^{i\lambda_o t} \qquad (14)$$

It is seen that total transverse rate is a vector rotating with frequency λ_o, which is the sum of the initial rate, ω_o, and the perturbation rate, ω'. The perturbation rate comprises two components. The $\beta\lambda$ component lies along ω_o, while the $(\omega^2 - \lambda^2)$ component is normal to ω_o. The effect of the $\beta\lambda$ component is to increase or decrease ω_o, while the $(\omega^2 - \lambda^2)$ component tends to merely "turn" ω_o. The essential change in the initial rate is expressed by

$$\omega_o\left\{1 - \left(\frac{m_I x_o^2}{A}\right)\frac{\lambda_o\lambda_I(\lambda_I - \Omega_I)^2}{\left[\omega_I^2 - \lambda_I^2\right]^2 + \beta_I^2\lambda_I^2}\left(\frac{\beta_I}{2}\right)t\right.$$

$$\left. - \left(\frac{m_{II} h_o^2}{A}\right)\frac{\lambda_o^3\lambda_{II}}{\left[\omega_{II}^2 - \lambda_{II}^2\right]^2 + \beta_{II}^2\lambda_{II}^2}\left(\frac{\beta_{II}}{2}\right)t\right\} \qquad (15)$$

Note that the initial rate is diminishing if

$$\lambda_I,\ \lambda_{II} > 0$$

If either λ_I or λ_{II} were negative, the sign of the change of ω_o would depend on the relative magnitude of the two time-varying terms.

Examining the oscillator-induced perturbation torques on body spin rates, from Equation 11 it is recalled that

$$\dot{\Omega}_I = \frac{2 m_I x_o}{C}\omega_o\dot{z}\cos\lambda_I t - \frac{m_I x_o}{C}\omega_o\lambda_o z\sin\lambda_I t$$

$$\dot{\Omega}_{II} = -\frac{m_{II} h_o}{I}\omega_o\lambda_o\rho\sin\lambda_{II} t$$

Substituting Equation 12 yields

$$\dot{\Omega}_I = -\frac{m_I x_o^2}{C}\frac{\omega_o^2(\lambda_I - \Omega_I)}{\left[\omega_I^2 - \lambda_I^2\right]^2 + \beta_I^2\lambda_I^2}\left\{\beta_I\lambda_I(\lambda_o\sin^2\lambda_I t - 2\lambda_I\cos^2\lambda_I t) + (\omega_I^2 - \lambda_I^2)(\lambda_o + 2\lambda_I)\sin\lambda_I t\cos\lambda_I t\right\} \qquad (16)$$

$$\dot{\Omega}_2 = \frac{m_{II} h_o^2}{I}\frac{\omega_o^2\lambda_o^2}{\left[\omega_{II}^2 - \lambda_{II}^2\right]^2 + \beta_{II}^2\lambda_{II}^2}\left\{\beta_{II}\lambda_{II}\sin^2\lambda_{II} t + (\omega_{II}^2 - \lambda_{II}^2)\sin\lambda_{II} t\cos\lambda_{II} t\right\}$$

Observe that the secular torque acting on the spin rate is due to the phase lag, $\beta\lambda$ term. If the dampers were "tuned" to the rates, λ_I, λ_{II} such that

$$(\omega_I - \lambda_I) = (\omega_{II} - \lambda_{II}) = 0$$

the effect of the oscillators would be entirely secular, contrary to the notions stated in Reference 4. Taking average values over nutation cycles gives

$$\bar{\dot{\Omega}}_I = \left(\frac{m_I x_o^2}{C}\right)\left(\frac{\beta_I}{2}\right)\frac{\lambda_I(\lambda_I - \Omega_I)^2}{[\omega_I^2 - \lambda_I^2]^2 + \beta_I^2\lambda_I^2}\cdot\omega_o^2$$

$$\bar{\dot{\Omega}}_{II} = \left(\frac{m_{II}h_o^2}{I}\right)\left(\frac{\beta_{II}}{2}\right)\frac{\lambda_{II}\lambda_o^2}{[\omega_{II}^2 - \lambda_{II}^2]^2 + \beta_{II}^2\lambda_{II}^2}\cdot\omega_o^2 \qquad (17)$$

Here, too, the signs of the spin rate changes are governed by λ_I and λ_{II}.

Solution About Small Nutation Angles

If the initial nutation angle is small such that

$$\frac{\omega_o}{\lambda_o} \ll 1$$

the nutation frequencies do not change appreciably during the nutation decay. In this case, it is appropriate to write

$$\omega(t) = \omega_o\, e^{-\left[\left(\frac{m_I x_o^2}{A}\right)\frac{\lambda_o\lambda_I(\lambda_I-\Omega_I)^2}{[\omega_I^2-\lambda_I^2]^2+\beta_I^2\lambda_I^2}\frac{\beta_I}{2} + \left(\frac{m_{II}h_o^2}{A}\right)\frac{\lambda_o^3\lambda_{II}}{[\omega_{II}^2-\lambda_{II}^2]^2+\beta_{II}^2\lambda_{II}^2}\frac{\beta_{II}}{2}\right]t}$$

This result has been verified by digital computer simulation of the exact equations. Excellent agreement was found when the previously stated assumptions were satisfied.

IV. COMPARISON WITH ENERGY ANALYSIS

To compare these results with the previous energy analysis, form

$$\dot{T}_I = -c_I\dot{z}^2 = -m_I\beta_I\dot{z}^2$$

$$\dot{T}_{II} = -c_{II}\dot{\rho}^2 = -m_{II}\beta_{II}\dot{\rho}^2$$

From Equation 12, $\dot{z}^2$ and $\dot{\rho}^2$ are obtained:

$$\dot{z}^2 = \left[\frac{x_o\omega_o(\lambda_I-\Omega_I)}{(\omega_I^2-\lambda_I^2)^2+\beta_I^2\lambda_I^2}\right]^2\lambda_I^2\left[\beta_I^2\lambda_I^2\cos^2\lambda_I t - 2\beta_I\lambda_I(\omega_I^2-\lambda_I^2)\sin\lambda_I t\cos\lambda_I t + (\omega_I^2-\lambda_I^2)^2\sin^2\lambda_I t\right]$$

$$\dot{\rho}^2 = \left[\frac{-h_o\omega_o\lambda}{(\omega_{II}^2-\lambda_{II}^2)^2+\beta_{II}^2\lambda_{II}^2}\right]^2\lambda_{II}^2\left[\beta_{II}^2\lambda_{II}^2\cos^2\lambda_{II} t - 2\beta_{II}\lambda_{II}(\omega_{II}^2-\lambda_{II}^2)\sin\lambda_{II} t\cos\lambda_{II} t + (\omega_{II}^2-\lambda_{II}^2)^2\sin^2\lambda_{II} t\right]$$

Taking average values over a nutation cycle,

$$\dot{T}_I = -\frac{m_I x_o^2\omega_o^2(\lambda_I-\Omega_I)^2}{[\omega_I^2-\lambda_I^2]^2+\beta_I^2\lambda_I^2}\cdot\lambda_I^2\cdot\left(\frac{\beta_I}{2}\right)$$

$$\dot{T}_{II} = -\frac{m_{II}h_o^2\omega_o^2\lambda_o^2}{[\omega_{II}^2-\lambda_{II}^2]^2+\beta_{II}^2\lambda_{II}^2}\cdot\lambda_{II}^2\cdot\left(\frac{\beta_{II}}{2}\right) \qquad (18)$$

Recalling from Equation 6 that

$$C\dot{\Omega}_I = -\frac{\dot{T}_I}{\lambda_I}$$

$$I\dot{\Omega}_{II} = -\frac{\dot{T}_{II}}{\lambda_{II}}$$

and substituting Equation 18 results in

$$\dot{\Omega}_I = \frac{m_I x_o^2}{C}\frac{\lambda_I(\lambda_I-\Omega_I)^2}{[\omega_I^2-\lambda_{II}^2]^2+\beta_I^2\lambda_I^2}\left(\frac{\beta_I}{2}\right)\omega_o^2$$

$$\dot{\Omega}_I = \left(\frac{m_{II}h_o^2}{I}\right)\frac{\lambda_{II}\lambda_o^2}{[\omega_{II}^2-\lambda_{II}^2]^2+\beta_{II}^2\lambda_{II}^2}\cdot\left(\frac{\beta_{II}}{2}\right)\omega_o^2$$

duplicating Equation 17. Writing Equation 7,

$$\dot{\omega} = \frac{\lambda_o}{A\omega_o}\left(\frac{\dot{T}_I}{\lambda_I} + \frac{\dot{T}_{II}}{\lambda_{II}}\right)$$

and substituting Equation 18 results in

$$\dot{\omega} = -\left(\frac{m_I x_o^2}{A}\right)\frac{\lambda_o\omega_o(\lambda_I - \Omega_I)^2\lambda_I}{[\omega_I^2 - \lambda_I^2]^2 + \beta_I^2\lambda_I^2}\left(\frac{\beta_I}{2}\right)$$

$$-\left(\frac{m_{II}h_o^2}{A}\right)\frac{\lambda_o^2\lambda_{II}\omega_o}{[\omega_{II}^2 - \lambda_{II}^2]^2 + \beta_{II}^2\lambda_{II}^2}\cdot\left(\frac{\beta_{II}}{2}\right)$$

duplicating Equation 15.

V. CONCLUDING REMARKS

The dynamic analysis indeed corroborates the vehicle rate changes predicted by the earlier energy analysis and illustrates its underlying assumptions. Also demonstrated are the inertial forces which sustain relative motion and the role of nutation frequencies, λ_I and λ_{II}. With the analysis as background, it is not surprising that the effect of a nutation damper depends on the body in which it is located; for its motion, and thus its reaction torque, is governed by the local nutation frequency which may be quite different in each body.

REFERENCES

1. V. D. Landon and B. Stewart, "Nutational Stability of an Axisymmetric Body Containing a Rotor," Journal of Spacecraft and Rockets, Volume 1, No. 6, 1964, pp. 682-684.
2. A. J. Iorillo, "Nutation Damping," Internal IDC, Hughes Aircraft Co., October 1964.
3. W. T. Thomson and G. S. Reiter, "Attitude Drift of Space Vehicles," Journal of Astronautical Sciences, Vol. 7, 1960, pp. 29-34.
4. W. F. Cartwright, R. D. Trueblood, and E. C. Massingill, "Circular Constraint Nutation Damper Analysis," GM Defense Research Laboratories Report TM 62-205, December 1961, General Motors Corporation.

DEVELOPMENT OF HUGHES GYROSTAT SYSTEM

ABSTRACT

This note describes results of theoretical and experimental research performed in the last several years which has led to the development of Hughes Gyrostat stabilization concept.

I. INTRODUCTION

The Hughes Gyrostat system is, generically, a spin-stabilized spacecraft with a despun platform. The unique feature of Gyrostat is that the platform is virtually unlimited in size. The system is not constrained to have the pancake shape demanded by the familiar inertia ratio criterion used to design current spinning satellites with or without despun platforms. Due to the "pancake" criterion, requiring spin about an axis of maximum inertia, present craft are limited in both overall length and despun platform size by launch vehicle shroud diameters. Also, since shrouds are longer than wide, the pancake constraint results in nonoptimum use of shroud volume.

Alternately, Gyrostat may be described as a rotor-stabilized spacecraft differing from present designs of this type in a fundamental way. Gyrostat is not constrained to have a perfectly rigid rotor, i.e., a metallic flywheel, dictated by the nutational stability criterion used to design satellites of this class. In essence, Gyrostat is the broadest application of spin stabilization. It bridges the gap between present nonrigid spinners with despun platforms and perfectly rigid rotor stabilized spacecraft. Free from the rigid rotor constraint, the rotor in Gyrostat is used to perform many functions in addition to effecting gyroscopic stability. Examples of some of these additional uses are:

- An apogee kick motor may be housed within the rotor and passively stabilized by its spin.
- The attitude and velocity control system may be spun, thereby requiring merely three jets for all axis control. The jet system spin also makes the spacecraft essentially insensitive to the torques induced by leaks since they are averaged out every spin cycle.
- Relatively simple attitude sensors may be rigidly mounted to the rotor and scan targets by virtue of spin. Pointing accuracy of 10 arcseconds may be achieved by using one rigidly mounted star scanner (a visible-light sensitive phototube located at the focal plane of a 2-inch telescope, weighing 8 pounds). For less demanding missions, the sensor would be an IR earth scanner.
- Solar cells may be fixed to the rotor.
- The rotor may also carry payload requiring spin, such as the ATS spin-scan meteorological camera.
- The rotor may act as a sun shield for electronics, permitting passive thermal control for most missions.

Further, since the rotor comprises a significant portion of the spacecraft, it has a high spin moment of inertia, and large gyroscopic stiffnesses may be achieved at very low spin rates (10 to 100 rpm).

In summary, Gyrostat provides a fully stabilized platform while maintaining features of well-proven spinner technology. In fact, all hardware aspects of Gyrostat have developmental roots in the Syncom and OSO programs. This hardware has been combined into a new configuration long recognized as attractively suited for many missions but heretofore considered dynamically unstable.

The Gyrostat concept evolved simply from the discovery that it is possible and practical to passively stabilize the spin of a nonrigid body about an axis of least inertia if the body contains a counterrotating element on which a nonrigid energy dissipation mechanism, a nutation damper, may be placed. In present Gyrostat designs (Figure 1) the counterrotating element carries payload as well, thus it is large. However, it need not be. For example, a quite small counterrotating box containing a nutation damper can be used to stabilize a large, slender spinning liquid rocket or could have been used to stabilize Explorer I had the principle been known at that time.

II. REVIEW OF THE DEVELOPMENT OF TWO-BODY THEORY

A study of the dynamics of two-body configurations was initiated at Hughes in early 1964. This study was motivated by the desire to add despun elements to Syncom satellites after the OSO program demonstrated that rotating elements could be operated in space for years. The object of the study was to determine whether stability of two-body configurations was governed by the well-known criterion for spinning mono-bodies. That is, a mono-body must be spun about its axis of greatest inertia. By simple extension of analysis used for mono-bodies, it was learned 1) that two-body stability does not necessarily require spin about a major axis and 2) that the distribution of energy dissipation between the two-bodies plays a role (Reference 1). This same conclusion was reached by Landon and Stewart at RCA in a paper which appeared at nearly the same time (Reference 2). Both of these works had an important shortcoming, however. To perform the simple extension of mono-body theory, both analyses were limited to the

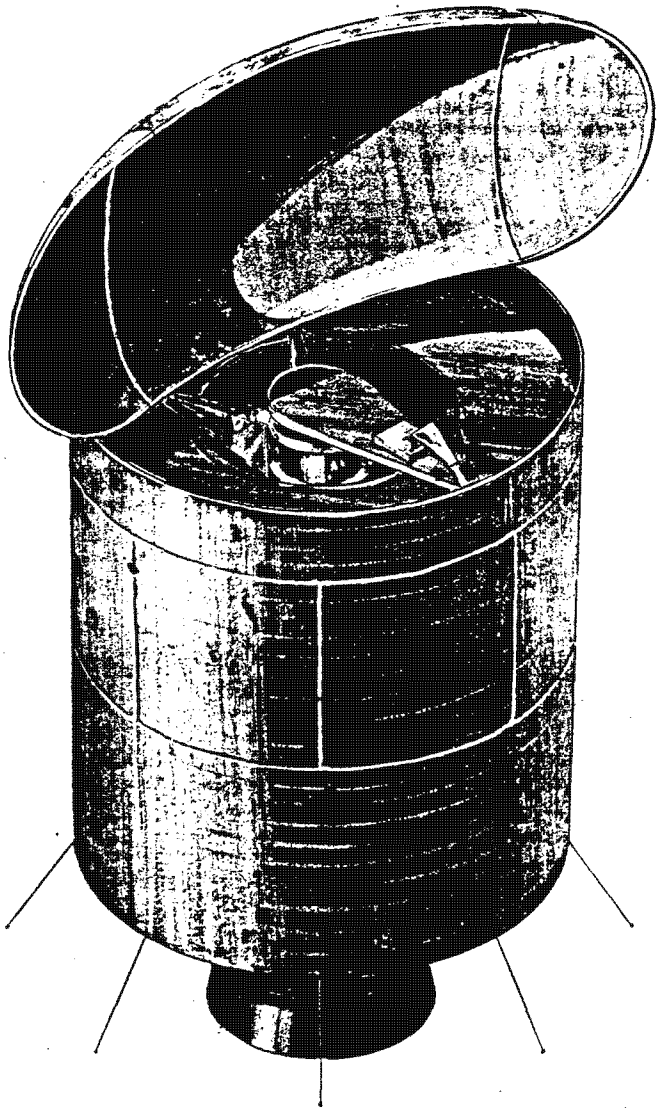

Figure 1. Typical Hughes Gyrostat System Design

special case of a two-body configuration wherein only one of the bodies is nonrigid. With this assumption, detailed quantitative consideration of poorly understood nonrigid effects (i.e., energy dissipation) could be avoided. The important results of these analyses are twofold: 1) if the spinning member is nonrigid, its spin moment of inertia must be greater than the combined configuration transverse moment of inertia, essentially the same as the inertia ratio criterion for mono-bodies; and 2) if the spinning member is perfectly rigid, a flywheel, the two-body configuration is practically free of inertia constraints. To attack the problem of a general two-body configuration wherein both bodies are nonrigid, it was clear that detailed understanding of the role of nonrigid effects was required.

By analyzing equations of motion of two-body systems with specific nonrigid elements, nutation dampers, physical understanding of the manner in which motion of dampers affected gross system motion was developed (Reference 1). The relationship between the amount of energy which a damper dissipated into a dash pot, for example, and gross sytem motion was learned. With this understanding of specific cases, the classical energy-sink method was reconstructed to deal with the general two-body nonrigid system (Reference 3). This energy-sink analysis is reproduced below.

III. GENERAL TWO-BODY ANALYSIS

The symmetric two-body system analyzed is illustrated in Figure 2. Except for rotation about the axis of symmetry, bodies I and II are rigidly joined. Only the nutational, or torque-free, motion is to be considered. The rates Ω_I and Ω_{II} are the spin rates of bodies I and II, respectively. The rate ω_o is the transverse or wobble rate of the combined system. The vector H is the system angular momentum vector and is thus the vector sum

$$\vec{H} = \overrightarrow{C\,\Omega_I + I\Omega_{II}} + \overrightarrow{A\omega_o} \qquad (1)$$

where

C, I ~ spin moments of inertia of bodies I and II, respectively

A ~ combined system transverse moment of inertia

For convenience without loss of generality,

$$C\,\Omega_I + I\,\Omega_I \geq 0$$

$$\omega_o \geq 0$$

This definition is tantamount to establishing a reference total momentum direction. Also, the spin and transverse moments are orthogonal.

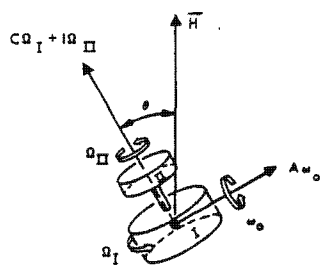

$$\tan\theta = \frac{A\omega_o}{C\Omega_I + I\Omega_{II}} = \frac{\omega_o}{\lambda_o}$$

Figure 2. Nutational Geometry Axisymmetric Two-Body Configuration

Since the nutation angle, θ, is directly related to the angular rates,

$$\tan\theta = \frac{A\,\omega_o}{C\,\Omega_I + I\,\Omega_{II}} \qquad (2)$$

nutational motion can be studied by considering angular rates alone. The question to be answered now is what is the change in these rates when energy is dissipated within the system. This does not mean frictional losses in the shaft coupling the two bodies but rather losses due to flexing structure and the like within the bodies during nutation. (In real systems, a servo loop-controlled motor acts to exactly counterbalance shaft friction. It is assumed here that the shaft is frictionless.)

If the system were lossless, perfectly rigid, the kinetic energy integral of the equations of motion would exist as

$$2T = A\,\omega_o^2 + C\,\Omega_I^2 + I\,\Omega_{II}^2 = \text{constant} \qquad (3)$$

Introducing internal dissipation, T is not a constant but a function of time. Equation 1 is then written as

$$\dot{T} = A\,\omega_o\dot{\omega}_o + C\,\Omega_I\,\dot{\Omega}_I + I\Omega_{II}\,\dot{\Omega}_{II} < 0 \qquad (4)$$

where $\dot{T}$ represents the total rate at which energy is dissipated and, by definition, is a negative quantity. Since the total dissipation is the sum of the dissipation in bodies I and II, let

$$\dot{T} = \dot{T}_I + \dot{T}_{II} = A\,\omega_o\dot{\omega}_o + C\,\Omega_I\,\dot{\Omega}_I + I\,\Omega_{II}\,\dot{\Omega}_{II} \qquad (5)$$

Considering now only the system motion due to dissipation and not due to exterior torques

$$\dot{\vec{H}} = 0 \qquad (6)$$

This is the statement of conservation of momentum. Equation 6 demands

$$\frac{d}{dt}\left\{(C\,\Omega_I + I\,\Omega_{II})^2 + (A\,\omega_o)^2\right\} = 0 \qquad (7)$$

or

$$(C\,\Omega_I + I\,\Omega_{II})\,(C\,\dot{\Omega}_I + I\,\dot{\Omega}_{II}) + A^2\,\omega_o\dot{\omega}_o = 0 \qquad (8)$$

With Equation 5, there are now two equations which the change in rates must satisfy. Rewriting them,

$$A\,\omega_o\dot{\omega}_o = \frac{C\,\Omega_I + I\,\Omega_{II}}{A}\left\{C\,\dot{\Omega}_I + I\,\dot{\Omega}_{II}\right\} \qquad (9)$$

$$\dot{T}_I + \dot{T}_{II} = A\,\omega_o\dot{\omega}_o + C\,\Omega_I\,\dot{\Omega}_I + I\,\dot{\Omega}_{II}\Omega_{II} < 0 \qquad (10)$$

Earlier analyses made simplifying assumptions for an obvious reason. There are three quantities of interest and only two equations. The simplification to a system wherein one body is perfectly rigid permits reduction to two quantities. For example, assuming body I to be rigid permits, after valid physical argument, letting $\dot{\Omega}_I,\ \dot{T}_I = 0$.

The present analysis, however, combines Equations 9 and 10 to form

$$\dot{T}_I + \dot{T}_{II} = -\left(\frac{C\,\Omega_I + I\,\Omega_{II}}{A} - \Omega_I\right) C\,\dot{\Omega}_I - \left(\frac{C\,\Omega_I + I\,\Omega_{II}}{A} - \Omega_{II}\right) I\,\dot{\Omega}_{II} \qquad (11)$$

With the background of earlier noted analyses of equations of motion of specific systems and a development of physical insight into the role of dissipation, Equation 11 was recognized as the sum of two equations:

$$C\,\dot{\Omega}_I = \frac{\dot{T}_I}{\lambda_I}, \qquad I\,\dot{\Omega}_{II} = -\frac{\dot{T}_{II}}{\lambda_{II}} \qquad (12)$$

where

$$\lambda_I = \frac{C\,\Omega_I + I\,\Omega_{II}}{A} - \Omega_I$$

$$\lambda_{II} = \frac{C\,\Omega_I + I\,\Omega_{II}}{A} - \Omega_{II}$$

Equations 12 relate the dissipation rates in each body to the change in spin rate of that body. As such, they are equations of motion. The quantities λ_I and λ_{II} are characteristic frequencies of motion of nonrigid elements within bodies I and II, respectively, when these elements are dissipating energy. Substituting Equation 12 into 9 results in

$$A\,\omega_o\dot{\omega}_o = \lambda_o\left(\frac{\dot{T}_I}{\lambda_I} + \frac{\dot{T}_{II}}{\lambda_{II}}\right) \qquad (13)$$

where

$$\lambda_o = \frac{C\,\Omega_I + I\,\Omega_{II}}{A}$$

which is, by definition, a positive quantity. The quantity λ_o is recognized as the total system nutation frequency. Equation 13 is a fundamental relation between the change in system wobble, $\dot{\omega}_o$, the energy dissipation rates within each body and system parameters. The question of system stability is equivalent to asking under what conditions an initial wobble rate, ω_o, subsides. For subsidence, $\dot{\omega}_o < 0$, the conditions are those which satisfy

$$\frac{\dot{T}_I}{\lambda_I} + \frac{\dot{T}_{II}}{\lambda_{II}} < 0 \qquad (14)$$

recognizing that λ_I and λ_{II} can be of either sign, depending on system parameters.

IV. INTERPRETATION OF RESULT

For a spinner with a despun platform, the relations stated in Equation 14 may be written

$$\frac{\dot{T}_s}{\lambda_s} + \frac{\dot{T}_p}{\lambda_p} < 0 \qquad (15)$$

where subscripts s and p refer to spinner and platform, respectively.

$$\lambda_s = \frac{I_s \Omega_s + I_p \Omega_p}{A} - \Omega_s$$

$$\lambda_p = \frac{I_s \Omega_s + I_p \Omega_p}{A} - \Omega_p$$

Assuming the spinner momentum is much larger than the platform spin momentum due to its nominal once per orbit rate, $\Omega_p \cong$ orbital rate,

$$\lambda_s \cong \frac{I_s \Omega_s}{A} - \Omega_s \cong \left(\frac{I_s}{A} - 1\right)\Omega_s \qquad (16)$$

$$\lambda_p \cong \frac{I_s \Omega_s}{A}$$

Substituting Equation 16 into Equation 15, the stability condition becomes

$$\frac{\dot{T}_p}{\left(\frac{I_s}{A}\right)} + \frac{\dot{T}_s}{\left(\frac{I_s}{A} - 1\right)} < 0 \qquad (17)$$

For a satellite like OSO, whose rotor spin moment of inertia is larger than the system transverse inertia, i.e.,

$$I_s > A$$

the condition cited in Equation 17 is satisfied independent of dissipation distribution. What this implies is that a damper may be placed on either the platform or spinner to dampen nutation.

For a satellite with a rigid flywheel, $\dot{T}_s = 0$, stability is assured practically independent of the ratio I_s/A.

For a Gyrostat design,

$$\frac{I_s}{A} < 1$$

and thus the quantity

$$\frac{\dot{T}_s}{\frac{I_s}{A} - 1} > 0$$

while

$$\frac{\dot{T}_p}{\frac{I_s}{A}} < 0$$

Stability of a Gyrostat design then requires

$$\left|\dot{T}_p\right| > \left|\left(\frac{I_s}{A}\right)\left(\frac{\dot{T}_s}{\frac{I_s}{A} - 1}\right)\right| \qquad (18)$$

For typical designs,

$$\frac{I_s}{A} < \frac{2}{3}$$

and thus

$$\frac{\dot{T}_p}{\dot{T}_s} > 2$$

or the dissipation rate on the platform must be at least two times the dissipation rate within the spinner. (As the inertia ratio decreases, the minimum dissipation rate required on the platform also decreases.)

V. PRACTICAL DESIGN CONSIDERATIONS

The relation of Equation 18 specifies the ratio of energy dissipation required for Gyrostat stability. The design requires quantitative measure of dissipation rates to ensure that this ratio is achieved. In typical Gyrostat systems, the principal source of destabilizing dissipation is liquid propellant slosh. An analytical model of fuel slosh dissipation was developed by D.D. Williams in mid-1965 for the Applications Technology Satellite program (Reference 4). Using his model, sloshing effects for typical propellant loads (100 to 200 pounds) were found to be small relative to the dissipation rate achievable with a small well-designed nutation damper (1 to 5 pounds). Thus, for Gyrostat designs,

$$\dot{T}_p >> \dot{T}_s$$

The primary design constraint for a damper becomes the need to dampen spacecraft wobbles due to booster separation, for example, within a reasonable time. Satisfying the relation in Equation 18 is then a natural fallout. The following computation will clarify this point.

VI. EXAMPLE COMPUTATION

A configuration designed to be launched into synchronous orbit by a Titan IIIC, about 1600 pounds, will be analyzed. The satellite consists of a nominal 10-foot diameter spinner weighing 800 pounds and carrying an 800-pound platform. Typical parameters for this configuration are

$$I = 400 \text{ slug-ft}^2$$

$$A = 1000 \text{ slug-ft}^2$$

$$\Omega_s = 100 \text{ rpm} \cong 10 \text{ rad/sec}$$

The principal energy dissipation mechanism in the spinner is the sloshing of 100 pounds of H_2O_2 reaction control fuel distributed in five spherical 12-inch diameter tanks. It is interesting to compute the destabilizing effect of this propellant loading if no nutation damper were present.

Williams shows that the energy dissipation rate of a sloshing, half-filled tank of fluid is given conservatively by

$$\dot{T} = \frac{1}{2}\left(\frac{M\ell}{I_f \lambda_s}\right)^2 \cdot \frac{B\, a_z^2}{\left(\frac{\omega_n^2}{\lambda_s^2} - 1\right)^2 + \left(\frac{B}{I_f \lambda_s}\right)^2} \qquad (19)$$

where, for the present case,

M = mass of fluid = 20 pounds

a = radius of tank = 0.5 foot

$I_f = 2/5\ M a^2 = 0.066$ slug-ft^2

$\ell = 3/8\ a = 0.187$ foot

$$\omega_n = \sqrt{\frac{15}{16} \cdot \frac{x_o \Omega_s^2}{a}} = 19.4 \text{ rad/sec}$$

(propellant natural frequency)

x_o = radial location of tank = 2 feet

$\lambda_s = (I/A - 1)\ \Omega_s = \lambda_s = 0.6\ \Omega_s = 6$ rad/sec (nutational forcing frequency)

$a_z = x_o\ (I/A - 2)\ \Omega_s \cdot \omega = 32\ \omega$ ft/sec^2

ω = transverse angular rate due to nutation

$$B = \frac{4}{3}\pi a^4 \left(\frac{\lambda_s \rho \mu}{2}\right)^{1/2} = 0.0039 \text{ ft-lb-sec}$$

ρ = density of fluid

$= 1.392 \frac{\text{gm}}{\text{cm}^3}$

μ = viscosity of fluid

$= 0.0134 \frac{\text{gm}}{\text{cm sec}}$

} 90 percent H_2O_2 at 18°C

For the present case,

$$\left(\frac{B}{I_f \lambda_s}\right)^2 << \left(\frac{\omega_n}{\lambda_s}\right)^4$$

The dissipation rate for <u>one</u> tank is then

$$\dot{T} \cong -2.0 \times 10^{-3}\, \omega^3 \frac{\text{ft-lb}}{\text{sec}}$$

For the vehicle with five tanks,

$$\dot{T}_s \cong -10^{-2}\, \omega^2 \frac{\text{ft-lb}}{\text{sec}}$$

If no nutation damper were present on the platform, the nutation amplitude divergence time constant due to fuel slosh would be obtained by solving Equation 13.

$$A\omega\dot{\omega} = \frac{\lambda_o}{\lambda_s} \cdot \dot{T}_s = \frac{\lambda_o}{\lambda_s} \cdot 10^{-2}\, \omega^2$$

or

$$\dot{\omega} = \frac{\lambda_o}{A\lambda_s} \cdot 10^{-2}\, \omega$$

The solution of this equation is

$$\omega(t) = \omega_o e^{\frac{\lambda_o}{A\lambda_s} 10^{-2} t}$$

The divergence time constant

$$\tau = \frac{A\lambda_s}{\lambda_o 10^{-2}} = 150{,}000 \text{ seconds} = 41.5 \text{ hours}$$

Clearly, the wobble buildup is slow. The reason for this slow buildup is understood by studying Equation 19. It is seen that the dissipation rate is proportional to

$$\left(\frac{\lambda_s^2}{\omega_n^2}\right)^2 \text{ or } \left(\frac{\lambda_s}{\omega_n}\right)^4 = \left(\frac{\text{nutational driving frequency}}{\text{natural sloshing frequency}}\right)^4$$

when this ratio is much less than unity. For the tank location and size analyzed, this ratio is

$$\left(\frac{6}{19.4}\right)^4 \cong 10^{-2}$$

This same frequency relationship holds true for a nutation damper. However, a damper's natural frequency is tuned to be close to the nutation frequency so that the ratio is nearly unity. Thus, a damper requires on the order of 1/100 the propellant mass to dissipate energy at this same rate. This is, in brief, the reason why a small damper can more than overcome large propellant loadings.

VII. TYPICAL DAMPER PARAMETERS

Rather than estimate the size of nutation damper which would just overcome the fuel slosh effect, the damper parameters required to provide a 1-minute damping time constant will be computed. Reference 3 shows that the damping time constant due to a simple spring-mass/dash pot damper located on the platform is given by

$$\tau_{\text{damping}} = \frac{A}{m h_o^2} \cdot \frac{2\beta}{\lambda_p^2} \qquad (20)$$

where

m = damper mass

h_o = damper location above the spacecraft center of mass

β = dash pot constant

This expression assumes the damper is tuned to be near resonance at λ_p. For the previous example,

$$\lambda_p = \frac{I_s \Omega_s}{A} = 4 \text{ rad/sec}$$

The spring constant, mass relationship required of the damper is then

$$\frac{k}{m} = \lambda_p^2 = 16 \text{ (rad/sec)}^2$$

where

k = spring restoring force/deflection ~ lb/in

Assuming the damper location is h_o = 3 feet and the damper mass is m = 4 pounds = 0.125 slug, τ_{damping} = 60 seconds requires a dash pot damping constant of β = 0.07 lb-sec/slug-ft, which is a nominal value, easily obtained. The spring constant required,

$$k = \lambda_p^2 m = 0.166 \text{ lb/in}$$

is also a nominal value, representing an easily wound spring. These computations illustrate that damper design is not particularly difficult.

VIII. CONCLUDING REMARKS

Previous sections describe preliminary analyses performed to establish feasibility and practicability of Gyrostat. Not presented are calculations of structural flexing effects. This is not dealt with since structural effects are also governed by the fourth power frequency relationship, and, for normal structural frequencies, typically greater than 10 cps (62.8 rad/sec), dissipation due to structural effects is several order of magnitude less than fuel slosh.

When the practical nature of Gyrostat was established, considerable effort was devoted to thoroughly consider all system aspects. Complete dynamic analysis of "real" systems, including an active despin servo loop coupling the spinner and platform, was performed using a digital computer simulation specifically designed for Gyrostat (Reference 5). Here, the dynamic integrity of a real system was established. Further, Reference 5 describes an air-bearing supported Gyrostat dynamic model which was fabricated and tested (Figure 3). The model corroborated theoretical conclusions. Reference 5 also compiles a number of analyses which treat the case of a Gyrostat with asymmetric platform complementing the analyses of References 1 and 3.

REFERENCES

1. A.J. Iorillo, "Nutation Damping," Hughes IDC 2230.14/69, October 1964.
2. V.D. Landon and B. Stewart, "Nutational Stability of an Axisymmetric Body Containing a Rotor," J. Spacecraft and Rockets 1, pp. 682-684, 1964.
3. A.J. Iorillo, "Nutation Damping Dynamics of Axisymmetric Rotor Stabilized Satellites," presented to ASME Winter Meeting, Chicago, Ill., November 1965.
4. D.D. Williams, "Estimates of Energy Dissipation and Nutation Damping Due to Fuel Sloshing in a Spherical Tank," Hughes IDC 2280.03/202, June 1965.
5. J.R. Velman, Attitude Dynamics of Dual-Spin Satellites, Hughes Report SSD 60419R, September 1966.

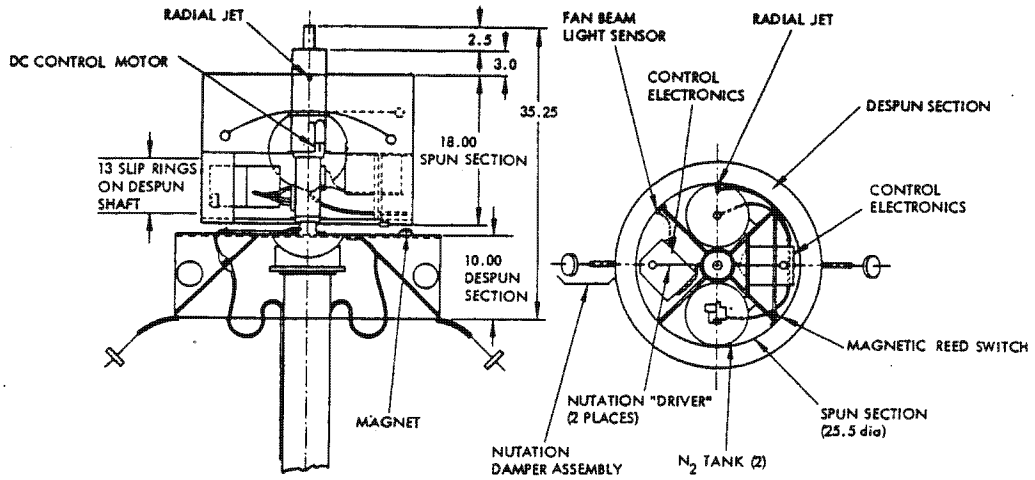

Figure 3. Hughes Gyrostat System Laboratory Model

PRECISION ASPECTS OF HUGHES GYROSTAT SYSTEM

ABSTRACT

A dual-spin satellite configuration is described which has been recently developed for application to missions requiring precise pointing of large payloads.

I. INTRODUCTION

The subject of this symposium, dual-spin satellites, is certainly not new. Yet for many years the dual-spin concept was not implemented as often as it might have been. Principally, because rotating electromechanical assemblies required in dual-spin designs were not felt to be reliable enough components. This feeling persisted even though an abundance of earth-based experience showed that such assemblies, comprising bearings, brushes, and sliprings, can be designed to function indefinitely. The reason for this fairly widespread opinion was lack of well-tested space lubrication techniques. Today, problems of maintaining long-lived lubrication in a vacuum environment are well understood and various solutions are available. Probably the best known of these is the Vackote system, developed by Ball Brothers Research Corporation, which has been demonstrated convincingly in their Orbiting Solar Observatory (OSO) satellites.

Certainly, OSO-I achievements did much to encourage our interest in adding a despun oriented platform to the basic Syncom spinning configuration with its integrated attitude, velocity, and passive thermal control systems. The simplicity and estimated cost of the resulting dual-spin system concept made it an attractive contender for missions requiring the steady pointing of payload.

It was apparent, however, that the nutational stability criterion demanding spin about an axis of maximum inertia severely restricted the capacity of the concept. The problem was that reasonable designs, whose spin diameters were booster shroud limited, could not carry large payload structures and still meet this inertia ratio rule (Reference 1). Recognizing that this criterion did not necessarily apply to dual-spin systems, an early attempt was made to determine specific criteria (Reference 2). Following the energy sink method used by Thompson, this analysis was confined to the special case of a system in which one of the bodies is rigid. It was shown that inertia constraints could be circumvented by using a rigid spinning member; i. e., a flywheel.

The concurrent Hughes attempt to solve the problem focused on the dynamics of specific nonrigid elements within nutating dual-spin systems and their reaction effects on gross system motion. Restricted in scope, this effort nonetheless provided some understanding of the roles which various parameters play during nutation. Finally, by informal reconstruction of the energy-sink method to cope with the excess variables of the general case which had caused prior confinement to special cases, criteria for nonrigid systems were obtained. Though lacking rigorous proof, the criteria were entirely consistent with the previously developed view of the physical process. The result indicated that dissipation mechanisms, such as propellant sloshing and structural flexing within a rotor, do cause destabilizing forces if the rotor spin inertia is not larger than configuration transverse inertias; however, similar mechanisms on the non-spinning platform always contribute stabilizing forces. Through detailed analysis of typical designs, it was discovered that normal structural flexing and sloshing of several hundred pounds of propellant within a rotor could be adequately compensated by a lightweight passive damper on the platform at arbitrarily small inertia ratios. Subsequent laboratory experiments and digital computer solution of exact equations of motion corroborated these findings (Reference 3).

The important conclusion of this work is that spinners should not be relegated to missions requiring small oriented payload as commonly assumed in system comparisons (Reference 4), but rather that their capacity can be made virtually unlimited quite easily. Further study of configurations with inertia ratios less than unity revealed another interesting property which is that they lend themselves naturally to precision pointing capability (Reference 5).

Current large spinner designs, with or without despun platforms, have inertia ratios marginally greater than unity in an attempt to package as much as possible into diameter-limited envelopes. The Application Technology Satellites for example have inertia ratios of 1.04, a nearly spherical inertial distribution. Consequently, they are difficult to dynamically balance with

precision. As a result, a despun platform on these vehicles experiences wobble of the order of 0.05 degree. Reasonably, this value has been assumed to be a practical limit of pointing accuracy for large spinners (Reference 4).

When freed of the inertia ratio constraint, there is an understandable tendency to design satellites which follow shroud volume forms, much longer than wide. Typical designs then have inertia ratios of 0.5 and lower. Since unbalance wobble is inversely proportional to the deviation from spherical symmetry, an order of magnitude improvement over current spinners is automatically realized. By adjusting satellite elements such that the overall transverse inertia is large, wobble can be reduced further to the arcsecond level. With the rotor so well balanced, satellite pointing capability is limited principally by factors common to any configuration such as sensor accuracy, overall alignment, and servo technology in general.

Based on the analyses referred to above, it was concluded that the concept pursued was not only inherently simpler but as capable as fully stabilized designs.

The first implementation of the system is the Tactical Communications Satellite presently under development (Figure 1). The satellite comprises a massive, oriented payload and a rotor which carries control and power systems as well as serving as a spinning sun-shield for electronics. The satellite may be described as either a spinner with a despun platform stabilized about an axis-of least inertia or a vehicle stabilized by a nonrigid rotor. In any event, this configuration is called the Hughes Gyrostat System (patent pending).

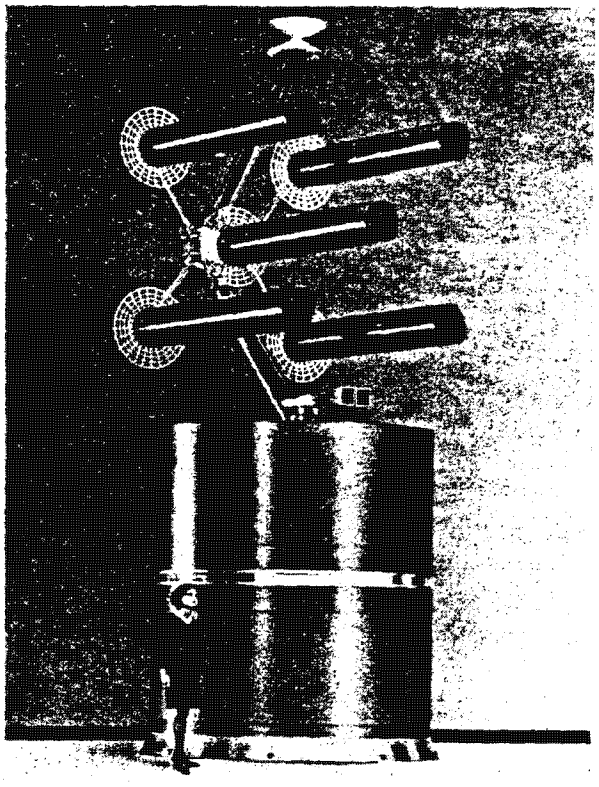

Figure 1. Tactical Communications Satellite

This note describes typical Gyrostat systems and discusses their performance as orbiting platforms.

II. SYSTEM DESCRIPTION

Several Gyrostat configurations are illustrated (Figures 2 and 3). The first is designed for a synchronous orbit mission and launch by an Atlas-Agena. The second is designed for a Titan launch. The common elements of these configurations are an oriented payload platform, a rotor which houses control and power subsystems, and a rotating interface for power and signal transfer as well as relative motion. Before describing the various subsystems, a typical mission profile is presented to fix ideas concerning functions which they must perform, Figure 4. The Atlas-Agena design is used for illustration because it fully exercises the various capabilities of the system.

Injected into a transfer orbit with perigee at about 100 n.mi. and apogee at synchronous altitude, the satellite is released with a conventional separation system and, almost simultaneously, the rotor is spun up with a one-shot propulsion system, either gas or solid. The despin servo keeps the platform from being dragged by bearing friction and acts to keep the platform at a low inertial rate required for nutation damper effectiveness. Stabilized by spin, the vehicle coasts to synchronous altitude. Gross velocity and attitude errors remnant from the injection phase can be corrected by ground command of a liquid propellant jet system. At apogee the kick motor is fired to form synchronous orbit. A maneuver is then ground commanded to precess the vehicle to an attitude normal to the orbit plane. The platform despin servo is then commanded to an earth-seeking mode and the mission can begin. Additional velocity errors are corrected to trim the orbit. (Except for despin servo operation, this same profile has been performed by all Syncom family satellites. All have been their own last stages. For Titan launches, a typical profile begins in synchronous orbit. The functions of achieving circular orbit and orienting the satellite along the north-south axis are accomplished before separation.)

The reaction system consists of three jets for attitude and velocity control. Mounted on the rotor, two jets are aligned parallel to the spin axis and the other normal to the spin axis along a rotor radius. When fired over a complete spin cycle, an axial jet provides north-south thrust without affecting attitude. When pulsed over a sector of a spin cycle, it causes a precessional control torque. The radial jet thrust acts through the vehicle center of mass and thus no torque results. Pulsed over a sector, it provides velocity control in any radial direction. (This same velocity and attitude control system concept has been used in all Hughes earth satellites.) Normally, the jet system is commanded at weekly intervals for stationkeeping and attitude trim maneuvers.

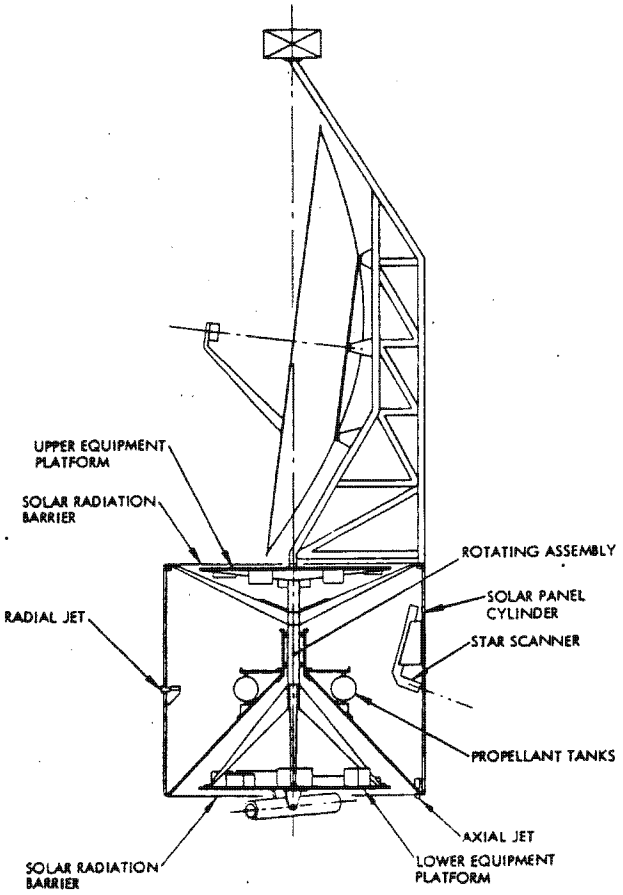

Figure 2. Typical Titan-Class Gyrostat Configuration

There are several distinct attitude-sensing functions. The platform control servo requires an angle error signal, and the ground operator or computer requires knowledge of satellite attitude to compute the sense and magnitude of reaction jet torquing commands. Further, satellite attitude data is required to process payload data.

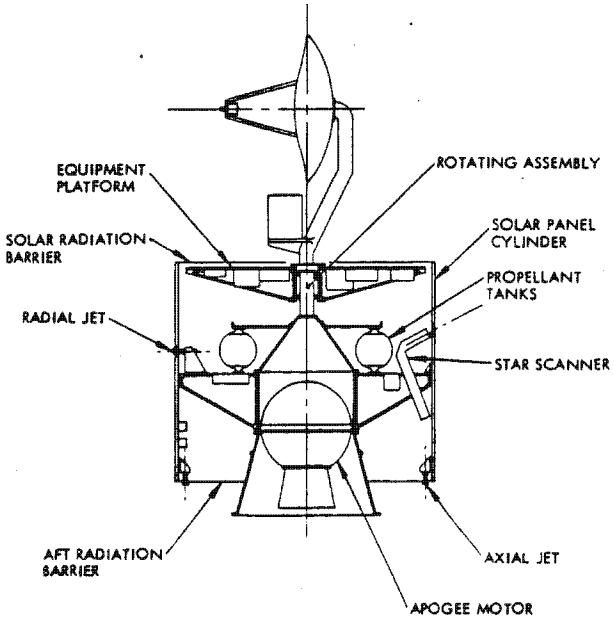

Figure 3. Typical Atlas-Agena-Class Gyrostat Configuration

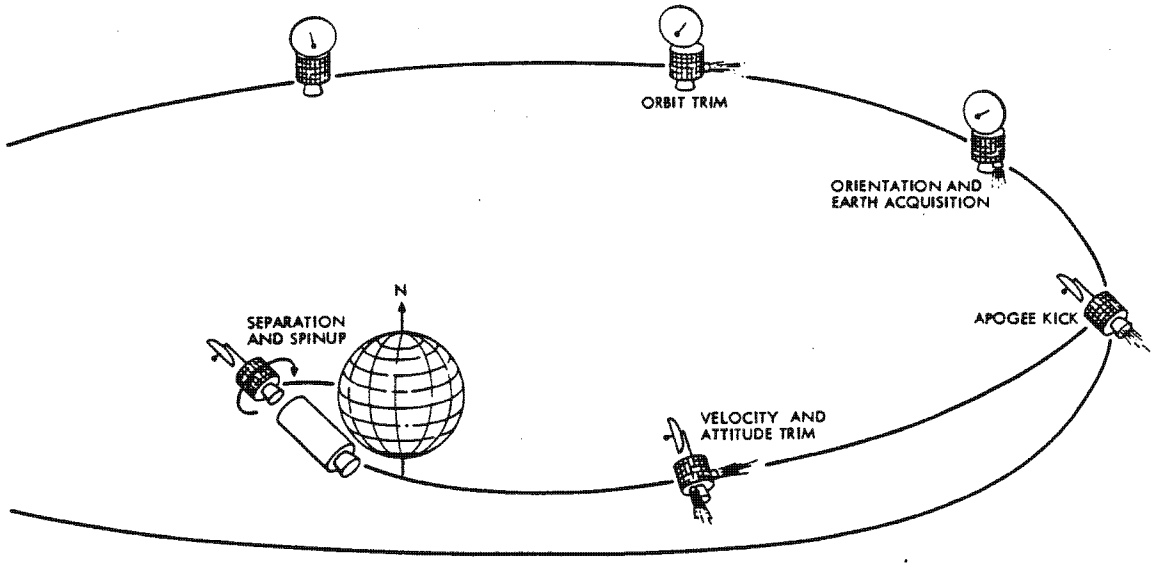

Figure 4. Typical Mission Profile

A single sensor, rigidly mounted to the rotor and thus scanned by spin, is all that is required to fulfill these needs. During the interval of one spin cycle, satellite attitude drift is less than 0.01 arcseconds. By scanning two or more inertial targets and by obtaining angular alignment relative to these targets, rotor attitude is determined in one cycle. Then to determine the inertial attitude of the platform, a measure of platform orientation relative to the rotor about the spin axis is necessary. Due to the considerable inertias of both platform and rotor, the relative motion between them remains constant enough to use a simple shaft encoder for measuring the relative angle. (Even for a 5-to 10-arcsecond system, a magnetic pip coil will usually suffice for this function.)

The outputs of both scanner and the pip coil are transmitted directly to ground for attitude determination and are also processed on board to derive a spin angle error for despin servo control.

For missions requiring nominal pointing accuracies of 0.20 degrees, a Tiros-type earth sensor can be used as the scanner for the despin loop, augmented by a simple sun sensor for complete determination.

For precision missions, a single star scanner is used for both despin control and attitude determination. A chevron-masked phototube and a lens system, (Figure 5) is effective as a star scanner. The geometry of star measurements is illustrated in Figure 6. Note that since the inertial attitude of the rotor is constant, the same stars, typically five in number, are scanned every spin cycle. No catalog or involved processing is required. A simple gating circuit is used to isolate the desired star pulse for the despin servo system.

The only active control system on board is the despin servo system whose principal elements are:

1) The scanning sensor and pip coil
2) Processing electronics
3) A servo motor

A typical system is illustrated in Figure 7. It is a fairly standard sampled data system with a rate loop for stable pointing and a supervision loop for directed pointing.

In the designs shown, electrical power is derived from solar panels which form the rotor cylinder and is continuously generated without active sun-pointing. Not a necessary feature of Gyrostat systems, rotor-mounted panels are generally preferred when the power required is consistent with a reasonable cylinder size and weight even though they are not as efficient as oriented panels. For missions with large power requirements, oriented panels (or other power sources) may be required. The system then would be a multi-spin configuration with a rotor, an earth-oriented platform, and a sun-oriented platform.

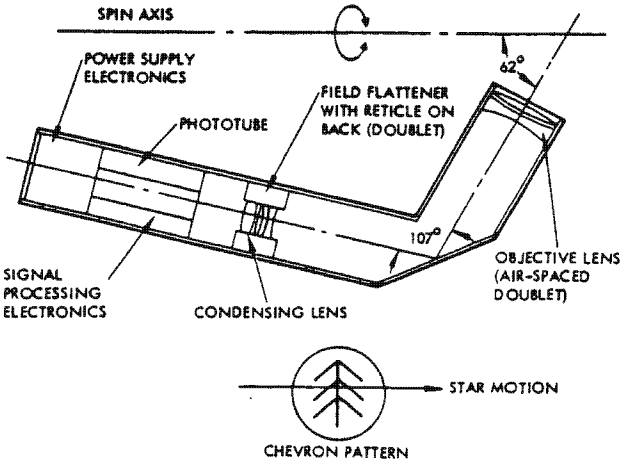

PHOTOMULTIPLIER	EMR-541-E
FIELD OF VIEW	4 deg
FOCAL LENGTH	10 in.
APERTURE DIAMETER	4 in.
RETICLE SLIT WIDTH	0.15 mr
BLUR DIAMETER	0.075 mr
SENSITIVITY	+2.6 MAGNITUDE
MINIMUM S/N	14 db
PULSE STABILITY	±5 arcseconds

Figure 5. Star Scanner

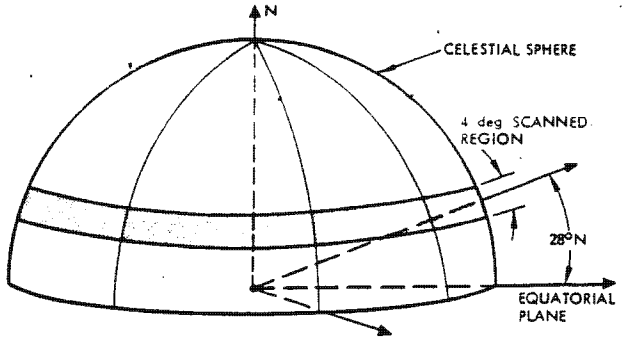

TARGET STARS	RIGHT ASCENSION	DECLINATION	MAGNITUDE
ALPHERATZ	1.51	28.89	2.00
β TAURI	80.77	28.58	1.64
POLLUX	115.57	28.12	1.15
α CORONAE	-126.75	26.84	2.23
β PEGASI	-14.23	27.88	2.61

Figure 6. Target Star Geometry

The rotating assembly consists of an outer housing, a pair of ball-bearings, a servo motor, a shaft, and a slipring-brush unit. The shaft protrudes through a labyrinth seal arrangement. Ten to twenty power slip rings are used both for redundancy and to keep the current flow per unit area at low levels. Signals for control and telemetry are crossed in a multiplexed digital bit stream through two rings.

III. SYSTEM PERFORMANCE CAPABILITY

Analyses are presented which are confined to aspects of system design that do not depend heavily on payload specification. Hence, structural, thermal control and power system analyses

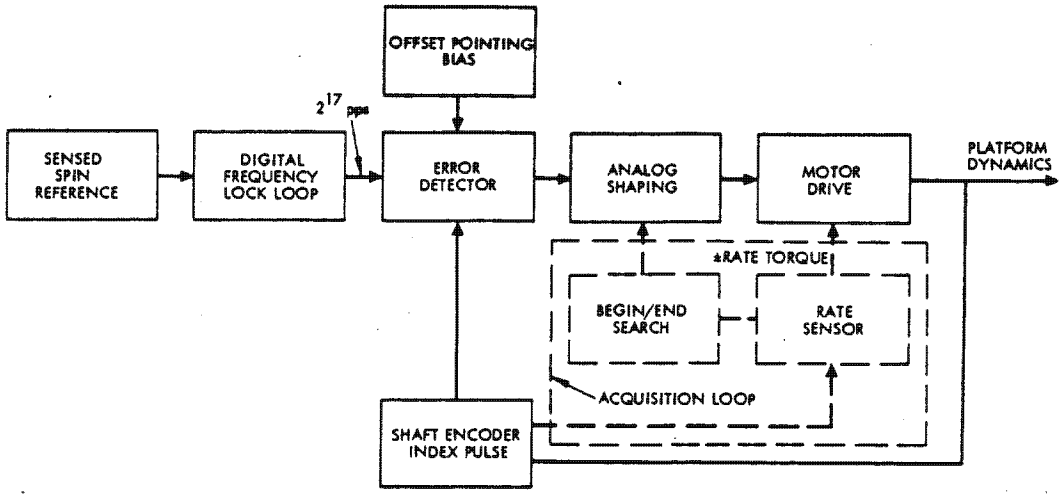

Figure 7. Platform Despin Control System

are not discussed. Rather, topics related to system performance as an orbiting payload bus which are not readily available elsewhere are considered. For brevity and current interest, high altitude missions are considered.

Nutational Stability

The stability criterion for nonrigid symmetric dual-spin systems is given by

$$\frac{\dot{T}_R}{\lambda_R} + \frac{\dot{T}_P}{\lambda_P} < 0 \qquad (1)$$

where

$\dot{T}_R$, $\dot{T}_P$ ≐ rates of energy dissipation in rotor and platform respectively, (always negative)

$$\lambda_R = \frac{I_R \Omega_R + I_P \Omega_P}{I_T} - \Omega_R$$

$$\lambda_P = \frac{I_R \Omega_R + I_P \Omega_P}{I_T} - \Omega_P$$

TABLE 1. TYPICAL PARAMETERS

Parameter	Atlas-Agena Class	Titan Class
Rotor spin inertia, I_R, slug-ft^2	300	400
Rotor tranverse inertia, I_{TR}, slug-ft^2	350	450
Configuration transverse inertia I_T, slug-ft^2	600	2000
Platform spin inertia, I_P, slug-ft^2	100	200
Rotor spin rate, Ω_R, rpm	60	60
Platform rate, Ω_P, rpm	10^{-3}	10^{-3}

For the case of a platform with low inertial rates (of the order of orbital rate), the momentum of the rotor is much larger than that of the platform. Hence, for practical purposes, the criterion becomes

$$\frac{\dot{T}_R}{\left(\frac{I_R}{I_T} - 1\right)} + \frac{\dot{T}_P}{\frac{I_R}{I_T}} < 0 \qquad (2)$$

The reduction of this criterion to the special cases of pure spinners and flywheel-stabilized designs is accomplished by letting $\dot{T}_P$ and $\dot{T}_R$ go to zero, respectively. For gyrostat systems, $I_T > I_R$, thus stability requires

$$|\dot{T}_P| > \left| \frac{I_R}{I_T} \left(\frac{\dot{T}_R}{\frac{I_R}{I_T} - 1} \right) \right| \qquad (3)$$

For example, at a ratio of 0.5, the dissipation rate on the platform must be greater than the dissipation rate within the rotor.

The principal rotor dissipation mechanism in the designs shown is the sloshing of propellant. Figure 8 illustrates dissipation due to sloshing within a single tank for several values of rotor spin. In a multitank system, these values are multiplied by the number of tanks. The contribution of structural flexing is normally an order of magnitude smaller than the peak slosh contribution.

It may be noted that the sloshing dissipation is low relative to the capability of nutation dampers normally used on spinners. Like the structural flexing mechanism, the natural frequency of slosh is typically greater than the nutation frequency which drives the motion by a factor of 4 or more. A damper is designed to be near resonance of the nutation frequency. Since the dissipation rate is proportional to

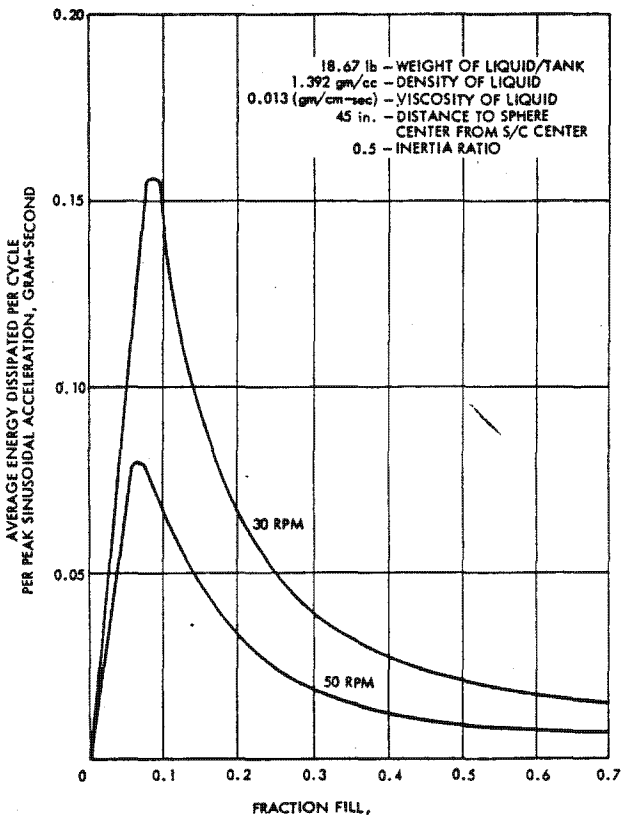

Figure 8. Energy Dissipation in Propellant Tank Versus Amount of Fluid in Tank For Different Spin Rates

$$\left(\frac{\lambda_R}{\omega_N}\right)^4 = \left(\frac{\text{nutational driving frequency}}{\text{natural frequency}}\right)^4$$

the slosh effect is expectedly low relative to an efficient damper.

For the designs shown, the destabilizing forces due to propellant slosh, if not compensated, cause nutation divergence time constants of 10 to 40 hours. A nutation damper, such as the pendulum damper on OSO-I, is designed to provide damping time constants of 5 to 20 minutes, which are more than sufficient to merely satisfy condition 3.

The stability criterion displayed here is for axisymmetric vehicles. For systems wherein the rotor is symmetric and the configuration is asymmetric, the average transverse inertia should be used (Reference 6).

Momentum Sizing

Typical system inertias are fallouts of structural and other system considerations. The spin rate is the only really free variable. Factors which influence spin rate selection are as follows:

- Desired resistance to exterior torques (attitude correction frequency)
- Required containment of motor thrust malalignment and axial jet offset
- Desired stiffness during possible payload slewing maneuvers
- Wearout life of bearings, brushes, and slipring s
- Energy required to create momentum (weight)

Depending on the mission, the minimum acceptable spin rate is from 5 to 10 rpm. Normally 60 rpm satisfies all objectives. Wearout life of the rotating assembly then is measured in tens of years.

With a momentum of 1800 to 2400 ft-lb-sec, the system is quite stiff. For high altitude missions, the largest exterior torque is due to solar pressure unbalance. Large system designs present average capture areas of the order of 200 ft^2. The resultant solar thrust is about 2×10^{-5} pounds. An attempt is made to minimize the distance between the average thrust center and the center of mass. However, a residual moment arm of 2 feet usually results. Hence, the drift rate induced is about 0.10 deg/day. Without correction, the attitude drift is in the form of a coning motion with a yearly period and maximum amplitude of 13 degrees. The drift over a spin cycle (one second) is less than 0.003 arcseconds. The nutation about this precession is of the same order. Short-term pointing stability is thus not limited by the rotor momentum capacity.

In missions that can tolerate a 0.5-degree pointing error, the drift is corrected weekly and the attitude is biased so that during the week the drift goes from +0.5 to -0.5 degree. For an absolute pointing accuracy of 10 arcseconds, a correction pulse every half hour is required. After drift calibration, maneuvers can be programmed onboard.

As an example of payload slewing effects, consider rotating a 10-foot diameter despun antenna 17 degrees (from the south pole to the north pole) in 1 minute. A typical antenna weighs 30 pounds including the feed and has an elevation inertia of about 10 slug-ft^2. The wobble or precession amplitude caused by the slewing is less than 0.002 degree. To decrease this effect an order of magnitude, a 10-minute time to cross the earth could be selected. Thus, reasonable mass motions on the despun platform are well contained by the rotor momentum.

Total weight of a cold gas blowdown system required for initial spin up is about 20 pounds, not unreasonable in a nominal 1500-pound design.

Reaction Jet System Sizing

Reaction jet system sizing consists of selecting jet thrust magnitudes and determining the

amount of propellant required for velocity and attitude control.

To precess the system 1 degree with an axial jet at a nominal 5-foot moment arm requires an 8-lb-sec total impulse. For the Titan class design, 1500 pounds, this may be expressed as an equivalent ΔV of 0.16 ft/sec/deg. To correct attitude drifts at the rate of 0.10 degree/day then requires about 6 ft/sec/year. This velocity increment is roughly equal to that required for in-plane stationkeeping in synchronous orbit, 7 ft/sec/year. (The velocity increment required to prevent orbit north-south precession is much larger at about 180 ft/sec/year.) Residual velocity errors at orbital injection are usually measured in hundreds of feet per second. Thus, even including spare attitude maneuver capability, attitude control requirements are small relative to velocity requirements.

Jet thrust level is governed chiefly by attitude correction resolution requirements. For normal missions, a 5-pound axial thrust at 5 feet suffices, giving a 0.03-degree-per-pulse resolution. For missions with a 10-arcsecond absolute pointing requirement, 0.1-pound thrust is needed at the 5-foot moment arm. Higher thrust levels could be used at lesser moment arms. In practice, a precision system might have large axial and radial jet thrustors for velocity control and a small additional axial jet for precision torquing. In any event, thrust size presents no special difficulty and common propellants may be used.

A detailed description of a typical system is presented in Reference 7.

Platform Wobble

This discussion presents sources of platform wobble and preliminary analyses intended to illustrate the feasibility of precision designs. Attention is focused on wobble due to unbalance, malalignment, imperfection of the rotating interface, and thermal deformation.

In essence, the platform is a stationary body to which a rotor is attached. Unbalance and malalignment of the rotor (Figure 9) cause wobble amplitude given by

$$\theta \cong \frac{(I_{xz} + mx\ell)}{I_R - I_T} \qquad (4)$$

where

I_{xz} = rotor product of inertia
m = rotor mass
ℓ = rotor center of mass displacement from total system center of mass
x = rotor center of mass deviation from spin axis

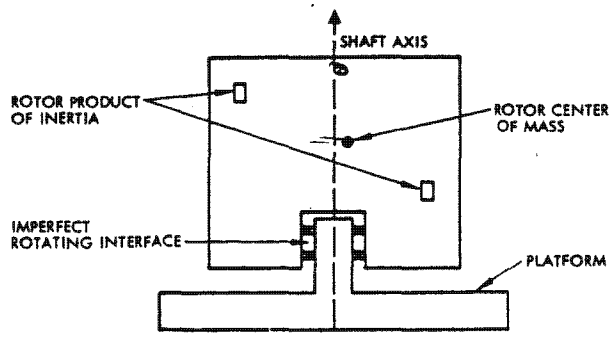

Figure 9. Platform Wobble Forces

Equation 4 is understood in terms of balancing procedures by noting that the torque measured with a rotor balancing machine is

$$\text{torque} = (I_{xz} + mxh)\,\Omega^2$$

where

Ω = rotor spin rate during balancing
h = rotor center of mass height above balancing machine torque reading instrumentation

For rotors less than 3000 pounds, spinning at 100 rpm, commercial equipment has a torque sensitivity of 0.2 ft-lb, which is equivalent to 2×10^{-3} slug-ft^2 of unbalance.

Assuming the rotor center of mass displacement from the satellite center of mass is equal to the rotor center of mass height above the balancing table transducers, the residual unbalance results in

$$\theta \cong \frac{2 \times 10^{-3}}{I_R - I_T} \text{ radians}$$

For the Atlas Agena class,

$$\theta \cong 1.2 \text{ arcseconds}$$

For the Titan class,

$$\theta < 0.3 \text{ arcsecond}$$

Another source of platform wobble is shaft runout in the rotating interface. Due principally

to ball asymmetries and bearing race ellipticity, the center of rotation of a ball bearing is not fixed with respect to the outer housing. In bearings suited for precision application (typically 4-inch ball bearings) the center of rotation deviation is less than 20×10^{-6} inches. (This value is quoted as a nonspecial tolerance by bearing manufacturers. With special ball selection procedures, it can be held to 5×10^{-6} inches.) For a bearing pair spaced 10 inches apart, this effect will cause runout of the order of 1 arcsecond. Manufacturing tolerance and alignment error buildups will also contribute to runout. A prototype rotating assembly was fabricated and subjected to vibration testing. Measurements were then made. The assembly demonstrated runout of the order of 3 arcseconds.

Due to thermal gradients within the rotor, balance and alignment are affected once in orbit (Figure 10). To illustrate the effect of thermally induced structural deformation, a simple model is analyzed. The rotor is assumed to be a hollow aluminum cylinder, 10 feet long and 10 feet in diameter. A constant temperature gradient of 2.5° C is assumed to exist across a diameter. (A 2.5° C gradient is a conservative upper bound for a rotor designed with minimization of internal gradients.)

The effects of the gradient are as follows: the center of mass is displaced from the shaft axis, and inertial symmetry about the axis is destroyed. The unbalance torque seen by the platform is

$$\{(I_S - I_{TR})\psi + m\delta\ell\}\Omega^2 \qquad (5)$$

The wobble is correspondingly given by

$$\theta \cong \frac{(I_R - I_{TR})\psi + m\delta\ell}{I_R - I_T} \qquad (6)$$

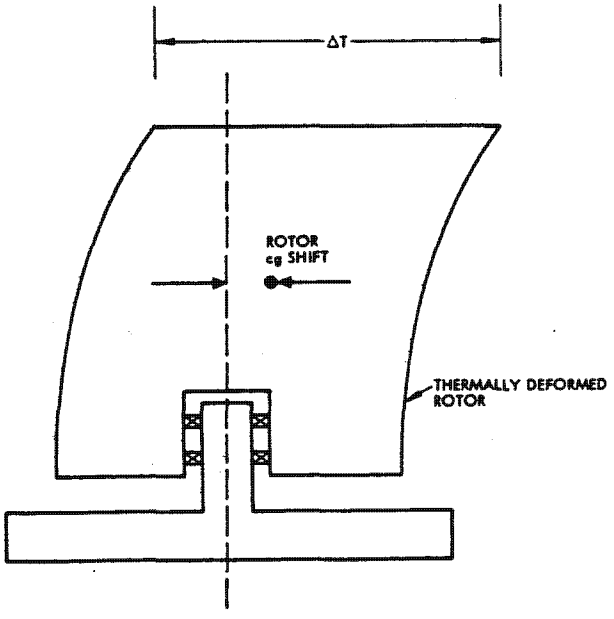

Figure 10. Rotor Deformation Due to Radial Thermal Gradient

where

ψ = effective rotation of rotor principal axis from shaft axis

m = rotor mass ≅ 15 slugs

δ = rotor mass displacement

ℓ = rotor mass axial distance from configuration center of mass ≅ 1 foot

The quantities δ and ψ are given approximately by

$$\delta \cong \left(\frac{K \Delta T}{2D}\right)\frac{L^2}{3}$$

$$\psi \cong \left(\frac{K \Delta T}{2D}\right)\frac{2L}{3}$$

where

K = coefficient of thermal expansion = 30×10^{-6} inch/inch/°C

ΔT = thermal gradient

D = rotor diameter ≅ 10 feet

L = rotor length ≅ 10 feet

The wobble induced is 1.7 arcseconds for the Agena design and 0.4 arcsecond for the Titan design.

The rotating interface will also experience thermal gradients. Due to the relative compactness of this unit, the gradient it experiences is small and its distortion does not cause significant malalignment or increase in bearing loading. This assertion has been checked in a vacuum thermal test using a prototype unit.

Structural relaxation in 0 g is computed to be less than the thermal effect for typical rotor constructions. (The 1-g relaxation is small relative to the 5-g centrifugal load which exists during balancing as well as in-orbit. Further, relaxation is axial and does not tend to distort radial symmetry.)

Care in matching propellant tank volumes and tank locations is required. Errors in tank location and differences in tank volumes cause unbalance with fluid utilization. Figure 11 illustrates malaligned, mismatched tank geometry. Assuming that deviations from nominal parameters are uncorrelated, the center of mass of a fluid in these tanks after a wet balancing procedure deviates from the spin axis an amount given by

$$\left[\left(\frac{3}{2}\frac{\delta R}{R_o}\right)^2 L_o^{\,2} + \left(\frac{\delta L}{2R_o}\right)^2 L_o^{\,2}\right]^{1/2} \cong d$$

Reasonable errors after careful tank selection are

$$\delta R = 0.001 \text{ inch}, \quad \delta L = 0.001 \text{ inch}$$

about the following nominal values

$$R_o = 12 \text{ inches}, \quad L_o = 24 \text{ inches}$$

The fluid center of mass deviation is thus

$$d \cong 4 \times 10^{-3} \text{ inches}$$

For a nominal initial propellant load of 17 pounds per tank, the mass unbalance which exists after propellant is totally expended is 2 oz-in. Typical tank center of mass separation from the configuration center of mass is 3 feet, with a resultant mass unbalance of 10^{-3} slug-ft^2, or wobble of 0.6 arcsecond for the ATLAS design and 0.15 arcsecond for the Titan design. Rotor inertial asymmetry due to this effect causes an order of magnitude less wobble.

Platform Despin Control and Calibration

The purpose of previous computations was to demonstrate the dynamic character of typical large systems. To the several arcsecond level, the rotor induces no significant platform wobble. Further, momentum is so large that attitude drift rate is extremely small.

Working on such a stable base, platform despin control can be effected to quite precise limits. In the stady-state condition, the principal function of a servo loop is to keep the relative rotation between rotor and platform constant. As in the case of wobble, the large inertias involved make this a relatively easy task. The principal disturbance affecting loop performance is drive motor and friction torque fluctuations.

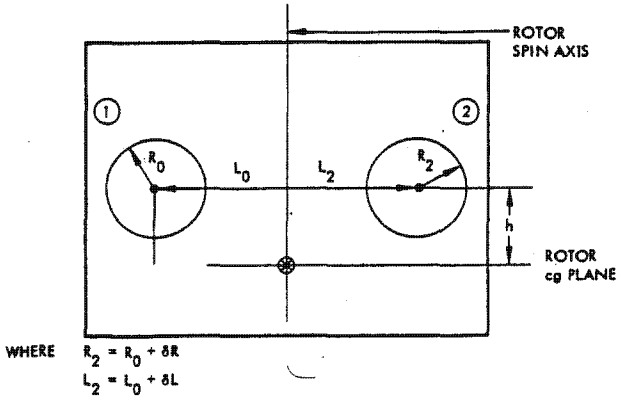

Figure 11. Mismatched, Malaligned Tank Geometry

Measurements with a prototype running at 55 rpm indicate that torque fluctuations are less than 0.025 ft-lb with frequencies greater than spin rate. Typical platforms with inertias of 100 to 200 slug-ft^2 respond with less than 2-arcsecond jitter amplitudes to these fluctuations even if they were at spin-rate.

Although pointing stability to the 5-arcsecond level is readily achieved, static pointing errors less than 0.02 degree are difficult to realize even with the star scanner. The principal limitation is system alignment. For missions which require precise absolute pointing, in-orbit calibration and adjustment is planned.

Here, the payload itself is used. Since optical payload (including many IR devices) can detect stars, natural calibration sources are the known star targets beyond the earth horizon. By slewing the platform away from the earth into the star field, it is found that at most wavelengths, dozens of stars can be detected in a single day. By comparing attitude determination system data with calibration data, malalignments and their variation can be determined and corrected through commanded adjustment of servo-loop parameters and the jet thrusting programmer. RF payload can be used for calibration by scanning known ground-based transmitters or receivers. In either case, system absolute pointing accuracy can normally be calibrated to the resolution of the payload requiring the accuracy.

IV. CONCLUDING REMARKS

We have attempted to stress several features of Gyrostat systems. Any size payload can be carried. By virtue of inertia and momentum, exceptional stabilization is afforded. And, using a relatively simple sensor, payloads can be pointed with extreme accuracy after in-orbit calibration and adjustment.

No active elements of the system are novel. The rotating interface, including motor drive, is patterned after OSO systems which have neither failed nor degraded in nearly 3 years of accumulated orbital life. The spinning reaction jet system concept has been used successfully on all Hughes satellites. The star-sensor phototube is similar to that still operating as a spinning meteorological camera on ATS-I. (Even the balancing equipment sensitivity cited was realized in the ATS program.)

Combined with the ability to use the passive thermal control concept and spinning power systems which have functioned perfectly in 10 years of accumulated Syncom family life, the Gyrostat system is believed to be inherently more reliable than any system yet advanced with comparable performance potential.

REFERENCES

(1) W. T. Thomson and G. S. Reiter, "Attitude Drift of Space Vehicles," Journal of Astronautical Sciences, Vol 7, 1960, pp. 29-34.

(2) V. D. Landon and B. Stewart, "Nutational Stability of an Axisymmetric Body Containing a Rotor," J. Spacecraft and Rockets 1, (1964) pp. 682-684.

(3) A. J. Iorillo, "Development of Hughes' Gyrostat System," Hughes Aircraft Company SSD 70012R, January 1967.

(4) H. Perkel, "Stabilite, A Three Axis Attitude Control System Utilizing a Single Reaction Wheel, AIAA Paper No. 66-307, May 2 through 4, 1966.

(5) "Precision Capability of Hughes' Gyrostat Systems," Hughes Aircraft Company SSD 70045R, February 1967.

(6) J. R. Velman, "Attitude Dynamics of Dual-Spin Satellites," Hughes Aircraft Company SSD 60419R, September 1966.

(7) R. J. McElvain and W. W. Porter, "Design Considerations for Spin Axis Control of Dual-Spin Spacecraft," presented at the Symposium on Attitude Stabilization and Control of Dual-Spin Spacecraft, El Segundo, California, 1-2 August 1967.